Nat. Hazards Earth Syst. Sci. Discuss., doi:10.5194/nhess-2017-73, 2017
Manuscript under review for journal Nat. Hazards Earth Syst. Sci.
Discussion started: 16 February 2017

Natural Hazards and Earth System Sciences
Open Access
Discussions

Sensitivity analysis and calibration of a dynamic physically-based slope stability model

Thomas Zieher[1,2], Martin Rutzinger[2], Barbara Schneider-Muntau[3], Frank Perzl[4], David Leidinger[5], Herbert Formayer[5], and Clemens Geitner[1]

[1]Institute of Geography, University of Innsbruck, Innrain 52f, 6020 Innsbruck, Austria
[2]Institute for Interdisciplinary Mountain Research, Austrian Academy of Sciences, Technikerstraße 21a, 6020 Innsbruck, Austria
[3]Unit of Geotechnical and Tunnel Engineering, Institute of Infrastructure, University of Innsbruck, Technikerstraße 13, 6020 Innsbruck, Austria
[4]Austrian Research and Training Centre for Forests, Natural Hazards and Landscape, Rennweg 1, 6020 Innsbruck, Austria
[5]Institute of Meteorology, University of Natural Resources and Life Sciences Vienna, Peter Jordan Straße 82, 1190 Vienna, Austria

Correspondence to: Thomas Zieher (thomas.zieher@uibk.ac.at)

Abstract. Physically-based modelling of slope stability at catchment scale is still a challenging task. Applying a physically-based model at such scale (1:10,000 to 1:50,000), parameters with a high impact on the model result should be calibrated to account for (i) the spatial variability of parameter values, (ii) shortcomings of the selected model, (iii) uncertainties of laboratory tests and field measurements or (iv) if parameters cannot be derived experimentally or measured in the field (e.g. calibration constants). While systematic parameter calibration is a common task in hydrological modelling, this is rarely done using physically-based slope stability models. In the present study a dynamic physically-based coupled hydrological/geomechanical slope stability model is calibrated based on a limited number of laboratory tests and a detailed multi-temporal shallow landslide inventory covering two landslide-triggering rainfall events in the Laternser valley, Vorarlberg (Austria). Sensitive parameters are identified based on a local one-at-a-time sensitivity analysis. These parameters (hydraulic conductivity, specific storage, effective angle of internal friction, effective cohesion) are systematically sampled and calibrated for a landslide-triggering rainfall event in August 2005. The identified model ensemble including 25 'behavioural model runs' with the highest portion of correctly predicted landslides and non-landslides is then validated with another landslide-triggering rainfall event in May 1999. The identified model ensemble correctly predicts the location and the supposed triggering timing of 73.5% of the observed landslides triggered in August 2005 and 91.5% of the observed landslides triggered in May 1999. Results of the model ensemble driven with raised precipitation input reveal a slight increase in areas potentially affected by slope failure. At the same time, the peak runoff increases more markedly, suggesting that precipitation intensities during the investigated landslide-triggering rainfall events were already close to or above the soil's infiltration capacity.

1 Introduction

Shallow landslides are abundant geomorphological phenomena in mountain regions of the world. The related processes are usually understood as translational sliding movement of soil material along a pre-defined slip surface at a depth of up to 2 m (Cruden and Varnes, 1996; Lateltin et al., 2005). In Austria, shallow landslides are typically triggered by heavy rainfalls (Andrecs et al., 2002; Markart et al., 2007; Zieher et al., 2016), causing damages to settlement objects and infrastructure as well as a loss of agricultural land. To prevent future impacts it is essential to identify potentially affected areas. For this task, various modelling techniques are currently applied, including (i) expert-based (e.g. Kienholz, 1977), (ii) statistically-based (e.g. Carrara et al., 1991) and (iii) physically-based approaches (e.g. Baum et al., 2010). The latter ones are typically based on the limit equilibrium concept employing physical laws to relate resisting to driving forces. Their result is a dimensionless factor of safety (FOS) which is a quantitative measure of slope stability. Many physically-based approaches include a hydrological and a geomechanical model element and can be further divided into (i) steady-state (e.g. Dietrich and Montgomery, 1998; Montgomery and Dietrich, 1994) and (ii) dynamic models (e.g. Baum et al., 2010; Crosta and Frattini, 2003). In contrast to steady-state models, dynamic models allow for the spatio-temporal assessment of hillslope hydrology and stability. Physically-based slope stability models can be upscaled to medium scale (1:10,000 to 1:50,000) using a raster-based geographical information system (GIS). However, spatially distributed models require data on the spatial distribution of the included parameters (van Westen et al., 2006).

Before applying a spatially distributed physically-based model, parameter values are often calibrated to minimize the difference between observations and simulation results. One way of achieving this, is to vary the model input parameter values in order to find optimal values or value ranges which yield a general agreement between observations and simulations (back calculation). This task is common in hydrological modelling involving a high-dimensional parameter space (e.g. Dobler and Pappenberger, 2013; Tang et al., 2007). The underlying principles also apply for physically-based slope stability models. Theoretically, a calibration is not necessary as long as the parameter values are based on a sufficient number of direct measurements or laboratory tests. However, a calibration is advisable (i) if the spatial distribution and variability of parameter values is unknown, (ii) to account for model shortcomings compared to the represented physical processes, (iii) to account for uncertainties of laboratory tests and field measurements or (iv) if parameter values cannot be derived experimentally or measured in the field (e.g. calibration constants). The calibration procedure should be based on physical reasoning and only involve sensitive parameters (i.e. parameters with a distinct impact on the model's outcome) (Bathurst et al., 2005; Wagener and Kollat, 2007). To identify sensitive parameters, a sensitivity analysis is usually performed. A simple, but often applied method is based on the local assessment (one representative raster cell) of the impact of systematic variations of one parameter at a time (OAT) on the model's results (e.g. Hammond et al., 1992). This method is also frequently used for parameter value calibration (e.g. Gioia et al., 2016; Salciarini et al., 2006). However, the OAT assessment of parameter sensitivity becomes unreliable with an increasing number of considered parameters, correlated parameters and non-linear model behaviour (Wagener and Kollat, 2007). As an alternative, global methods which cover the whole parameter space can overcome this drawback (Dobler and Pappenberger, 2013; Tang et al., 2007). Their main disadvantage is the high computational effort usually requiring a high performance computing cluster (HPCC). Depending on the sampling technique a multitude of parameter value combinations is tested and evaluated based on observations. However, instead of identifying a single parameter set which explains the observations best, an ensemble of 'behavioural model runs' is often used for the final prediction. These model runs are in general agreement with the observations while their disagreement reflects model uncertainty (Bathurst et al., 2005; Wagener and Kollat, 2007).

In the present study, the parameters of a revised form of the spatially distributed dynamic physically-based slope stability model TRIGRS 2.0 (Transient Rainfall Infiltration and Grid-Based Regional Slope-Stability Analysis; Baum et al., 2008, 2010) are systematically tested and calibrated. The four main steps of the analysis are shown in Fig. 1. First, sensitive parameters of the revised model are identified with a local OAT sensitivity analysis. The tested parameter space is derived from a limited number of laboratory tests and respective literature. Then, the four identified sensitive parameters (hydraulic conductivity, specific storage, effective inner angle of friction, effective cohesion) are systematically sampled and calibrated considering each parameter value combination for the whole catchment area (global approach). The best 25 'behavioural model runs' are identified which optimally predict the location and the supposed triggering timing of observed shallow landslides triggered during a rainfall event in August 2005. The predictive performance of this model ensemble is then tested for another landslide-triggering rainfall event in May 1999. Finally, the model ensemble is re-run with positively scaled input precipitation maps to give an estimate of expectable impacts of increasing precipitation intensities on slope stability.

The objectives of the present study are:

1. To identify sensitive parameters of the revised dynamic physically-based slope stability model TRIGRS 2.0
2. To present a procedure for a global parameter calibration (model identification) for a landslide-triggering rainfall event in August 2005, validated with another rainfall event in May 1999
3. To evaluate the capability of the identified model ensemble for quantifying potential changes in slope stability associated with increasing precipitation intensity

2 Study area

The study area is located in the Laternser valley in Vorarlberg, the westernmost province of Austria (Fig. 2a). It covers the catchment area (52.1 km^2) of the river Frutz, a tributary of the Rhine river. The valley extends about 13 km in east-west direction following the strike angle of the Bregenzerwald Mountains. Its highest point is the Hoher Freschen (2004 m) at the head of the valley. The outlet at approximately 500 m is characterized by a steeply incised gorge. In the Laternser valley about half of the catchment area is covered by forest (2001: 51.0%, 2006: 50.9%). A majority of the forest stands are composed of fir (*Abies alba* Miller) and spruce (*Picea abies* (L.) Karsten) with beech (*Fagus sylvatica* L.) occurring below 1300 m (Amann et al., 2014). Around 1.2% of the catchment area is occupied by settlements and infrastructure. The remaining area is predominantly used as hay meadow or pasture or a combination of both.

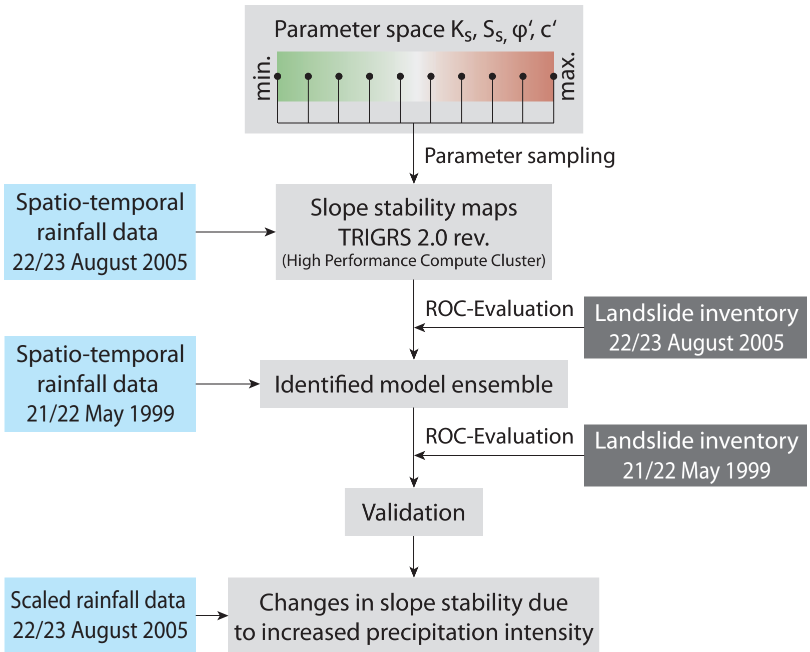

Figure 1. Workflow with the main steps of the analysis.

2.1 Geology

The Laternser valley is built up by different tectonic units. Helvetic nappes in the western and northern part of the valley include competent limestones (e.g. Schrattenkalk, Seewerkalk) and marls with calcareous layers (e.g. Drusbergschichten). To the south-east ultrahelvetic nappes are superimposed which are mainly built up of clayey marls and shales (e.g. Leimernmergel). On top in the south-east of the catchment, penninic nappes build up more than half of the valley. These nappes include mainly sandstones (e.g. Reiselsberger Sandstein, Planknerbrückenserie) and thinly layered marls (e.g. Piesenkopfschichten) (Friebe, 2007; Heissel et al., 1967; Oberhauser, 1982, 1998). Wide-spread till deposits and hillside debris cover more than 57% of the catchment area. These units are overly susceptible to shallow landsliding (Zieher et al., 2016). In numerous cases subglacial till is reported to act as impermeable layer and slip surface for the unconsolidated material on top. Furthermore, marls of the ultrahelvetic nappes as well as less competent sandstones of the penninic nappes are particularly susceptible to shallow landsliding (Zieher et al., 2016).

2.2 Climate

Oceanic air masses advected from the north-west dominate the warm temperate climate of Vorarlberg. On the fringe of the Alps in northern Vorarlberg precipitation amounts are higher due to blocking of the inflowing air masses (Werner and Auer, 2001b, a). Because of the valley's orientation, it is prone to north and north-westerly weather conditions. At Innerlaterns station (location mapped in Fig. 2c) the mean annual precipitation sum (period 1981–2010) exceeds 1800 mm a^{-1}. Considering

Nat. Hazards Earth Syst. Sci. Discuss., doi:10.5194/nhess-2017-73, 2017
Manuscript under review for journal Nat. Hazards Earth Syst. Sci.
Discussion started: 16 February 2017

Natural Hazards and Earth System Sciences
Open Access
Discussions

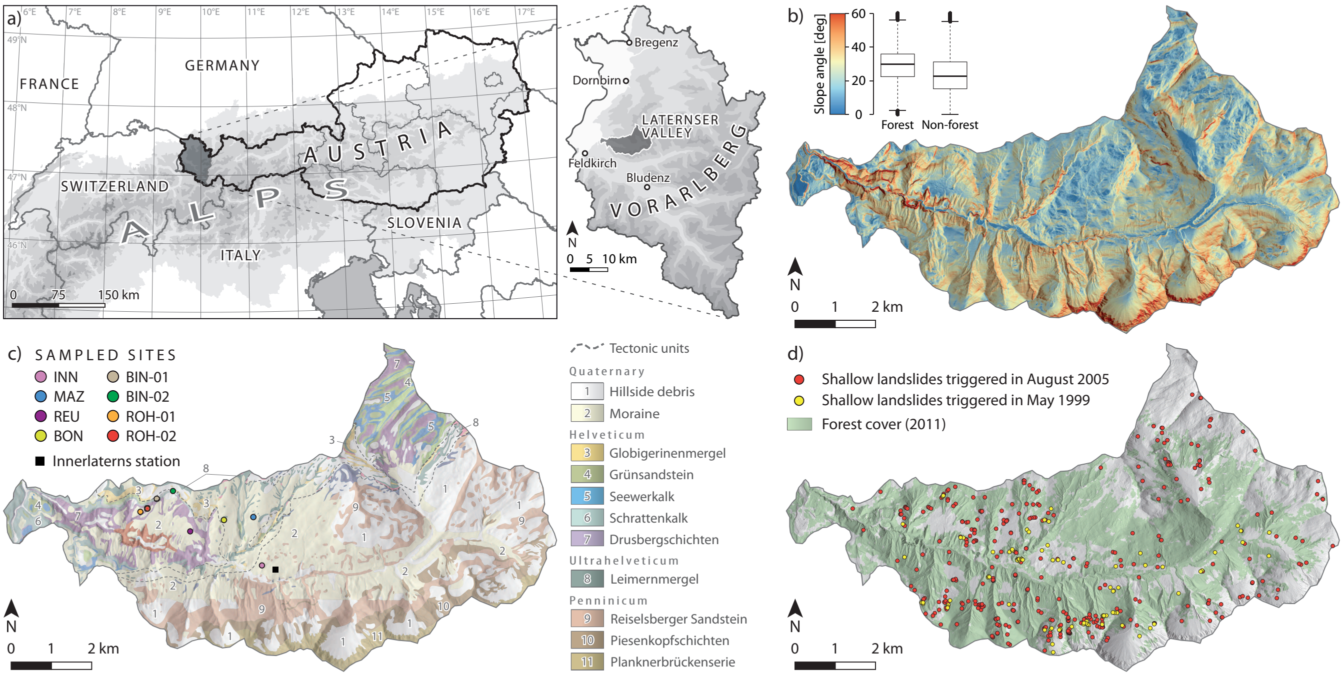

Figure 2. Location of the Laternser valley (a), slope angle map (b), geological map with sampled sites (c) and shallow landslide inventory (d). The slope angle map is based on a digital terrain model derived from airborne laser scanning (ALS) in 2011, serving as input data for modelling (resampled to a spatial resolution of 10 m). The boxplots show the slope angle distribution for forest and non-forest areas. In the geological map only geological units covering more than 1% of the catchment area are listed in the legend (Data source: Heissel et al., 1967; Oberhauser, 1982). The shallow landslide inventory shows landslides triggered by the rainfall events in May 1999 (82; yellow) and August 2005 (356; red) occurring on undisturbed hillside slopes (Zieher et al., 2016). The areas covered by forest were derived from ALS data acquired in 2011.

a potential evaporation in Vorarlberg in the order of 600 mm a^{-1} (Werner and Auer, 2001a), a year-round high amount of seepage water can be assumed.

At the synoptic scale the landslide-triggering rainfall events in May 1999 and August 2005 occurred in the course of so-called Vb weather situations (van Bebber, 1891; Formayer and Kromp-Kolb, 2009). Such synoptic meteorological situations are characterized by a low forming south of the Alps, subsequently moving to the North-East. The moisture taken up over the Mediterranean and Adriatic Sea is transported to East-Central Europe, potentially causing heavy rainfalls in large parts of Austria (Seibert et al., 2007).

2.3 Landslide-triggering rainfall events

Figure 3a,b shows the daily and cumulative deviation of precipitation from the long-term mean (1981–2010) covering one year before the landslide-triggering rainfall event in May 1999 and August 2005 respectively. For the period of June 1998 to

January 1999 the cumulative deviation of precipitation was in total balanced including a dry August and a wet September and October (Fig. 3a). Afterwards, particularly the second half of February 1999 was exceptionally wet. Locally, fresh snow depth exceeded two meters within three days leading to catastrophic snow avalanches (Bollinger et al., 2000; Heumader, 2000). In March and April 1999 the precipitation amount corresponded to the long-term mean, but precipitation in February an April provided an elevated level of the cumulative deviation. From May 11 to May 14 a rainfall event with a total sum of 144.4 mm occurred. No shallow landslides are reported for this event. However, increased soil moisture must be expected before the onset of the landslide-triggering rainfall event on May 21/22 with a total sum between 134.0 mm at Frastanz station and 212.8 mm at Thüringen station (Fig. 3c).

Monthly precipitation sums from November 2004 to June 2005 generally fell below the long-term mean except for February and May (Fig. 3b). Therefore it can be expected that no exceptional antecedent soil moisture preceded the rainfall event in August. However, the amount of precipitation in July and the first half of August corresponds to the long-term mean. Therefore, no exceptionally dry conditions preceded the landslide-triggering rainfall event. After days with repeated minor rainfalls a phase of intense precipitation started on August 22. At Innerlaterns station the 24 hour cumulative sum amounted up to 244 mm. The highest precipitation intensity was recorded in the late evening on August 22 and during the night hours (21 to 22 pm: 19.4 mm h^{-1}). The triggering time of four landslides was reconstructed from protocols of the local voluntary fire brigade (Fig. 3d). Most landslides occurred in the course of the night from August 22/23.

3 Materials and Methods

3.1 Shallow landslide inventory

A comprehensive shallow landslide inventory was compiled for the catchment area of the Laternser valley (Zieher et al., 2016). The inventory is based on the systematic interpretation of nine orthophoto series covering the period from 1950–2012. Landslide mapping was aided by digital terrain models (DTMs) derived from two ALS campaigns and their differential digital terrain model (dDTM). In addition, data from two field surveys conducted immediately after two landslide-triggering rainfall events in May 1999 and August 2005 and associated archive data was included in the inventory. In total, 82 shallow landslides attributed to the rainfall event in May 1999 and 356 shallow landslides triggered in August 2005 were used for this study (Fig. 2d). Only rainfall-triggered shallow landslides which occurred on undisturbed hillside slopes were considered which account for $3/4$ of the observed landslides for both rainfall events. Observed shallow landslides on other slope types may involve additional causative factors for slope failure which are not included in the model (e.g. weakened foot slope). Of the considered landslides, 28 (34.1%; May 1999) and 88 (24.7%; August 2005) are located within forests.

3.2 TRIGRS 2.0 model

The dynamic, physically-based coupled hydrological/geomechanical model TRIGRS 2.0 was developed by Baum et al. (2008, 2010) and is written in the Fortran programming language (USGS, 2016). TRIGRS 2.0 is based on a raster environment and

Nat. Hazards Earth Syst. Sci. Discuss., doi:10.5194/nhess-2017-73, 2017
Manuscript under review for journal Nat. Hazards Earth Syst. Sci.
Discussion started: 16 February 2017

Natural Hazards and Earth System Sciences
Open Access
Discussions

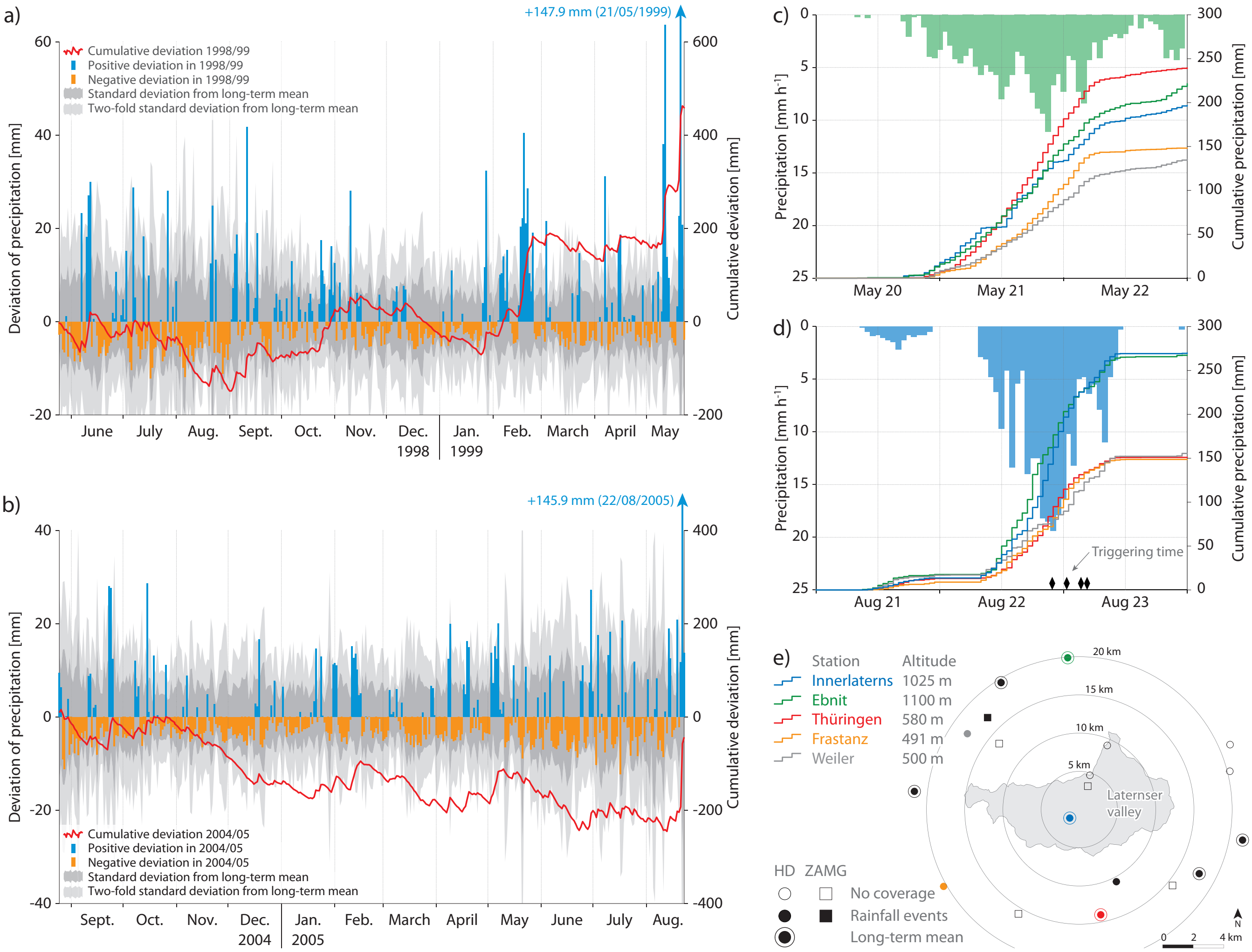

Figure 3. Landslide-triggering rainfall events in the Laternser valley on 21/22 May 1999 (a,c) and 22/23 August 2005 (b,d). The map (e) shows the considered meteorological stations. Regional mean daily (7:00–7:00) and cumulative deviation of precipitation from the long-term mean (1981–2010) are shown for the period of one year before the rainfall events (a,b). Cumulative precipitation for three days covering the landslide-triggering rainfall events are shown for meteorological stations within and surrounding the Laternser valley (c,d). Hourly precipitation sums are shown for Ebnit station in May 1999 (c) because at Innerlaterns station missing values are present in the respective hourly time series. Estimated triggering times of four shallow landslides were derived from protocols by the voluntary fire brigade. Data source: Hydrographic Service of Vorarlberg (HD), Central Institute for Meteorology and Geodynamics (ZAMG).

implements a hydrological model element (a runoff model and two types of infiltration models) and a geomechanical model element (infinite slope stability model). It is suitable for modelling the spatio-temporal progression of slope stability in the course of rainfall events with a duration of up to a few days (Baum et al., 2010).

In the model, the infiltration process and associated effects on slope stability are computed dynamically for each raster cell. Runoff R_d is routed downslope from raster cells where the precipitation intensity P plus the incoming runoff R_u from adjacent raster cells above exceeds the infiltration capacity (equal to the hydraulic conductivity K_s; Baum et al., 2008):

$$R_d = \begin{cases} P + R_u - K_s & \text{if } P + R_u - K_s \geq 0 \\ 0 & \text{if } P + R_u - K_s < 0 \end{cases} \tag{1}$$

However, the amount of runoff is not passed on to the next time step. The available amount of water ready for infiltration on each raster cell is passed on to the infiltration model. For tension-saturated initial conditions a generalized pore pressure diffusion model after Iverson (2000) can be applied. The predictive performance of Iverson's model has been tested in the Laternser valley at plot scale (Zieher et al., 2017). For unsaturated conditions an analytical solution for unsaturated flow following Srivastava and Yeh (1991) can be applied. However, the exponential model describing the soil water retention curve (Gardner, 1958) used for linearising Richard's equation is considered suitable for coarse-grained materials (Baum et al., 2008) and hence not suitable for the application in the Laternser valley. The details of the infiltration models have been presented in previous studies (e.g., Baum et al., 2010; Iverson, 2000; Kim et al., 2013; Park et al., 2013; Salciarini et al., 2006). The result of both infiltration models is the evolution of pore pressures with depth and time as response to the infiltration of time-varying precipitation. Pore pressures $\psi(d,t)$ are passed on to the infinite slope stability model relating driving to resisting stresses (factor of safety; FOS):

$$FOS(d,t) = \frac{\tan\varphi'}{\tan\beta} + \frac{c' - \psi(d,t)\cdot\gamma_w\cdot\tan\varphi'}{\gamma_s\cdot d\cdot\sin\beta\cdot\cos\beta} \tag{2}$$

where d [m] is the vertical depth (positive in downward direction), t [s] is time, φ' [deg] is the effective angle of internal friction, β [deg] is the slope angle, c' [Pa] is the effective cohesion per unit area, γ_w (9.81 N m^{-3}) is the unit weight of water and γ_s [N m^{-3}] is the unit weight of soil. Raster cells where the FOS falls below 1 are considered slope failures. Each cell with a $FOS < 1$ represents a single shallow landslide (Milledge et al., 2012). The model's results are FOS maps showing a quantitative measure of slope stability in space and time.

However, the original version of TRIGRS 2.0 does not account for effects of vegetation. Kim et al. (2013) extended the model to include vegetation effects on hydrology and slope stability. They conclude that root reinforcement and tree surcharge can affect slope stability while interception has only minor effects during landslide-triggering rainfall events. Following Kim et al. (2013), lateral root cohesion c_r [Pa] and tree surcharge s_t [Pa] were added to Eq. (2):

$$FOS(d,t) = \frac{\tan\varphi'}{\tan\beta} + \frac{c' + c_r - \psi(d,t)\cdot\gamma_w\cdot\tan\varphi'}{(s_t + \gamma_s\cdot d)\cdot\sin\beta\cdot\cos\beta} \tag{3}$$

Instead of adding a constant value for c_r (e.g. Kim et al., 2013), a linear decrease of c_r with depth up to a given rooting depth d_r [m] was assumed, accounting for the distribution of roots with depth as observed in other studies (e.g. Bischetti et al., 2005,

Table 1. Parameters for the revised TRIGRS 2.0 model and parameter values considered in previous studies. DEM: digital elevation model, K_s: saturated hydraulic conductivity. *revised form of TRIGRS 1.0.

Parameter	Unit	Salciarini et al. (2006)	Zizioli et al. (2013)	Vieira et al. (2010)	Park et al. (2013)	Kim et al. (2013)*
Precipitation intensity P	m s^{-1}	Station data	Station data	Station data	Station data	Station data
Slope angle β	Degree	DEM (5×5 m)	DEM (10×10 m)	DEM (2×2 m)	DEM (10×10 m)	DEM (5×5 m)
Regolith depth d_{max}	m	Function of slope angle	Geomorphologically indexed model	Constant value (1.0, 2.0 and 3.0 m)	Constant value (2.0 m)	Spline interpolation of measurements
Initial depth of the water table d_{wi}	m	0, 25, 50 and 100% of regolith depth	0.75 m below the surface	At regolith depth	At regolith depth	At regolith depth
Background infiltration rate I_z	m s^{-1}	-	-	1.00×10^{-9}	$0.01 \times K_s$	4.50×10^{-9}
Eff. angle of internal friction φ'	Degree	18.00–40.00	22.00–33.70	34.00	29.63	34.00
Effective cohesion c'	kPa	4.00–100.00	0.00–10.00	1.00; 6.00	10.17	5.20
Sat. hydraulic conductivity K_s	m s^{-1}	$10^{-8} - 10^{-4}$	$1.50 \times 10^{-5} - 1.00 \times 10^{-4}$	1.00×10^{-6}	1.30×10^{-5}	4.50×10^{-5}
Hydraulic diffusivity D_0	m^2 s^{-1}	-	-	5.5×10^{-5}	$200 \times K_s$	-
Unit weight of soil γ	kPa	18.00–22.00	17.46–19.91	17.10; 14.30	18.38	14.71
Root cohesion c_r	kPa	-	-	-	-	3.0
Tree surcharge s_t	kPa	-	-	-	-	2.9
Rooting depth d_r	m	-	-	-	-	-
Number of property zones		5	4	1	1	1

2009). If the rooting depth exceeds the regolith depth, c_r is only considered down to the regolith/bedrock interface (roots are not expected to penetrate the bedrock). For the revised form of TRIGRS 2.0, three additional parameters (c_r, s_t and d_r) must be given. The three parameters are allowed to vary spatially and can be prepared as parameter maps.

3.3 Model parameters

Table 1 shows the required parameters and their values considered in previous studies applying the original TRIGRS model (Version 1.0 and 2.0) and a revised form (Kim et al., 2013). In the cited studies, the time-varying precipitation intensities are derived from meteorological stations in or nearby the study area. The slope angle maps are calculated using DEMs (based on interpolated contour lines) of various spatial resolutions. Regolith depth maps are prepared as a function of the slope angle (Salciarini et al., 2006), by using a geomorphologically indexed model (Zizioli et al., 2013), a spline interpolation of direct measurements (Kim et al., 2013) and spatially constant values (Park et al., 2013; Vieira et al., 2010). The initial depth of the water table d_{wi} (positive in downward direction) is assumed to be either at the regolith/bedrock interface (Kim et al., 2013; Park et al., 2013; Vieira et al., 2010) or at a depth relative to it (Salciarini et al., 2006; Zizioli et al., 2013). For the background infiltration rate describing a steady-state infiltration component, constant values (e.g. Kim et al., 2013; Vieira et al., 2010) or multiples of K_s (e.g. Park et al., 2013) have been used.

For the landslide-triggering rainfall events considered in the present study, hourly precipitation maps were prepared covering the whole province of Vorarlberg. Based on hourly precipitation records from available meteorological stations throughout the province hourly precipitation maps were generated using a spline interpolation. Figure 4 shows the respective time series and the resulting cumulative precipitation maps for the Laternser valley. The temporal course of the precipitation intensities differs

Nat. Hazards Earth Syst. Sci. Discuss., doi:10.5194/nhess-2017-73, 2017
Manuscript under review for journal Nat. Hazards Earth Syst. Sci.
Discussion started: 16 February 2017

distinctively (August 2005: short and intense; May 1999: prolonged and less intense), while cumulative precipitation sums over the considered duration are in the same order (May 1999: 263 mm; August 2005: 252 mm). For modelling the temporal evolution of slope stability, FOS maps were computed for nine (May 1999; Fig. 4a) and seven (August 2005; Fig. 4c) time steps of nine hours to completely cover both rainfall events.

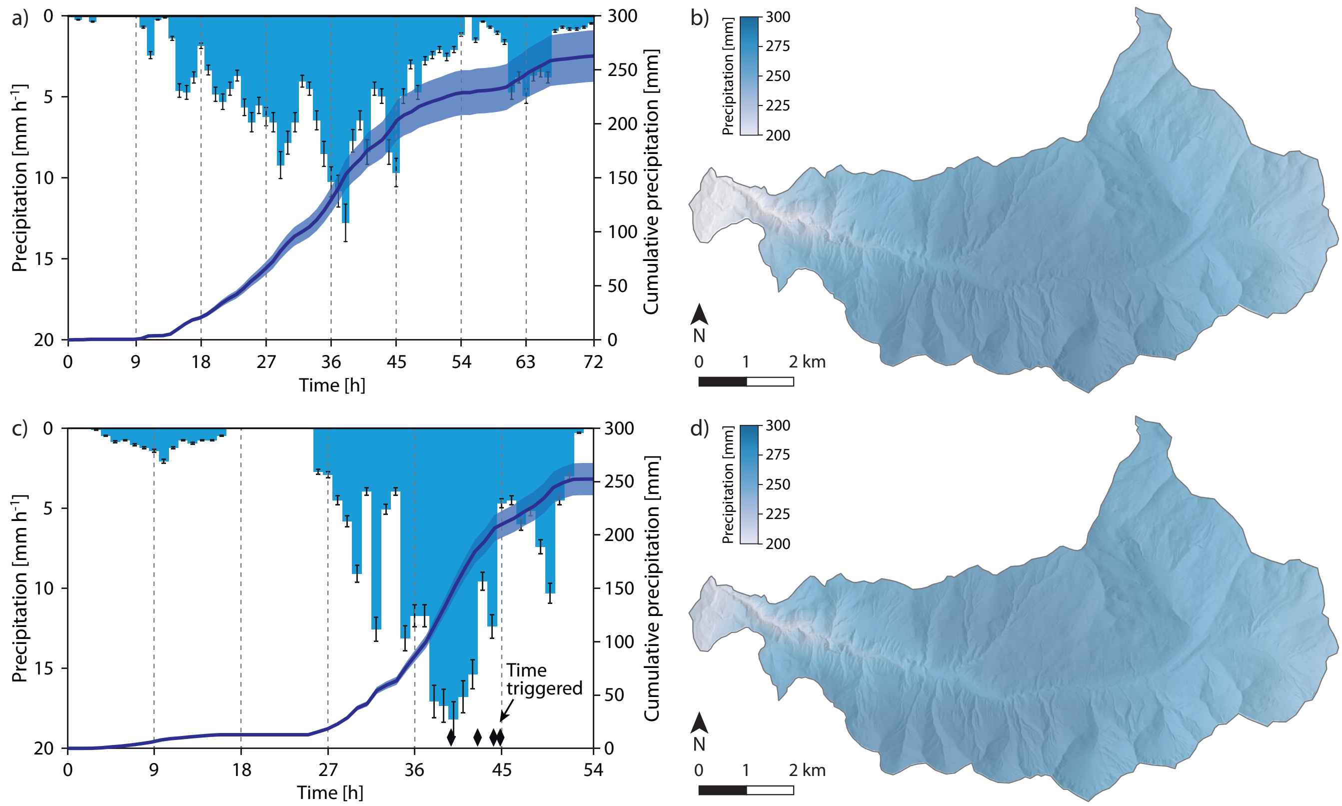

Figure 4. Hourly precipitation time series (a, c) and spatially interpolated precipitation sums (b,d) for the duration of the landslide-triggering rainfall events in 1999 (a,b; 20 May, 07:00–23 May, 07:00) and 2005 (c,d; August 21, 07:00–August 23, 12:00). The error bars and the shading for the cumulative precipitation sum in (a) and (c) indicate the range of the interpolated hourly precipitation sums within the catchment area.

The required slope angle map (Fig. 2b) was derived area-wide from a DTM after Wood (1996). The DTM was generated with ALS data acquired in 2011 with a reported accuracy of 10 cm in horizontal and 7.5 cm in vertical direction (Wiedenhöft and Vatslid, 2014). The data quality of the DTM from 2011 surpasses the quality of the DTM from 2004 particularly in areas covered by forest. The spatial resolution of the prepared parameter maps was set to 10 m with regard to the most abundant size of observed landslide scar areas, which is in the order of 100 m^2 (Zieher et al., 2016). Furthermore the chosen spatial resolution was considered a compromise between the topographical representation of the surface, the computational efficiency for the modelling and the required minimum length-to-depth ratio (in the order of 8:1) for the application of the infinite slope stability model (Milledge et al., 2012).

Nat. Hazards Earth Syst. Sci. Discuss., doi:10.5194/nhess-2017-73, 2017
Manuscript under review for journal Nat. Hazards Earth Syst. Sci.
Discussion started: 16 February 2017

Regolith depth, also referred to as soil depth (e.g. Lanni et al., 2013) or soil thickness (e.g. Catani et al., 2010; Segoni et al., 2012) is still one of the most difficult and laborious parameter to measure at catchment scale, yet crucial for physically-based modelling of slope stability (Dietrich et al., 1995; Lanni et al., 2012; Segoni et al., 2012). It is defined as the thickness of unconsolidated material covering the earth's surface, i.e. the depth from surface to bedrock (Fairbridge, 1968). Regolith depth can be assessed by (i) direct measurements (e.g. Lanni et al., 2012; Wiegand et al., 2013), (ii) means of geophysics (e.g. Davis and Annan, 1989; Sass, 2007) or modelling (e.g. Dietrich et al., 1995; Heimsath et al., 1997). Furthermore, the depth of past landslides can be derived from multi-temporal remotely sensed elevation data (Zieher et al., 2016). For regolith depth mapping, regression models correlating regolith depth to either elevation, slope angle or other derivatives were used in previous case studies on shallow landslide susceptibility (Baum et al., 2010; Lanni et al., 2012; Salciarini et al., 2006; Segoni et al., 2012). For the assessment of regolith depth in the Laternser valley, 126 dynamic cone penetration tests (DCPTs) were conducted along four transects. A lightweight dynamic cone penetrometer comprising a hammer of 10 kg dropped from a height of 0.5 m onto an anvil of 6 kg was used (e.g. Wiegand et al., 2013). Following ÖNORM EN ISO 22476-2:2012, the number of strokes for penetrating vertical increments of 10 cm was recorded in the field. After completing 50 strokes the penetration tests were stopped if the penetrated increment was less than 10 cm (ÖNORM EN ISO 22476-2:2012). The final depth was recorded to the nearest centimetre with the maximum detectable depth of 6.0 m exceeded only once. Furthermore, the maximum vertical depths of 96 shallow landslides triggered on 21/22 May 1999 and of 249 shallow landslides triggered on 22/23 August 2005 are available for validation (Fig. 5b). The landslide depths were measured in the field after the triggering event in May 1999 (Andrecs et al., 2002) and derived from the analysis of a dDTM for the landslides triggered in August 2005 (Zieher et al., 2016). The final depths of the DCPTs were used to train generalized linear models (GLMs) with local morphometric parameters as predictors including elevation, slope angle, minimum and maximum curvature (Wood, 1996) and the topographic wetness index (Beven and Kirkby, 1979). A stepwise backward predictor selection revealed a linear model with the slope angle yielding the best agreement with the cumulative landslide depths from 1999 and 2005 (Fig. 5a). It outperforms the curvature and the combined slope angle/curvature model particularly for depths below 2.0 m. The resulting empirical relationship for regolith depth d_{max} and the slope angle β is

$$d_{max} = \begin{cases} 3.028 - 0.049 \cdot \beta & \text{for } 0.0° \leq \beta < 61.8° \\ 0.0 & \text{for } \beta \geq 61.8° \end{cases} \quad (4)$$

The derived regolith depth map (Fig. 5b) also matches the field observation, that on slopes which are inclined more than approximately 60° the surficial cover of unconsolidated material is of minor depth or not present at all. Furthermore, on very steep slopes there is a transition from sliding to toppling and falling as the predominant types of failures (Baum et al., 2010).

For the derivation of the geotechnical and hydrological parameter values suitable for the Laternser valley, a limited number of laboratory tests were conducted. On the south-facing slopes of the study area geotechnical samples were collected from eight sites where shallow landslides had been triggered in 1999 (BIN-2), 2002 (ROH-01), 2005 (BIN-01, BON, MAZ, REU, ROH-02) and 2013 (INN) close to populated areas in the Laternser valley (Fig. 2c). The abbreviations were chosen according

Nat. Hazards Earth Syst. Sci. Discuss., doi:10.5194/nhess-2017-73, 2017
Manuscript under review for journal Nat. Hazards Earth Syst. Sci.
Discussion started: 16 February 2017

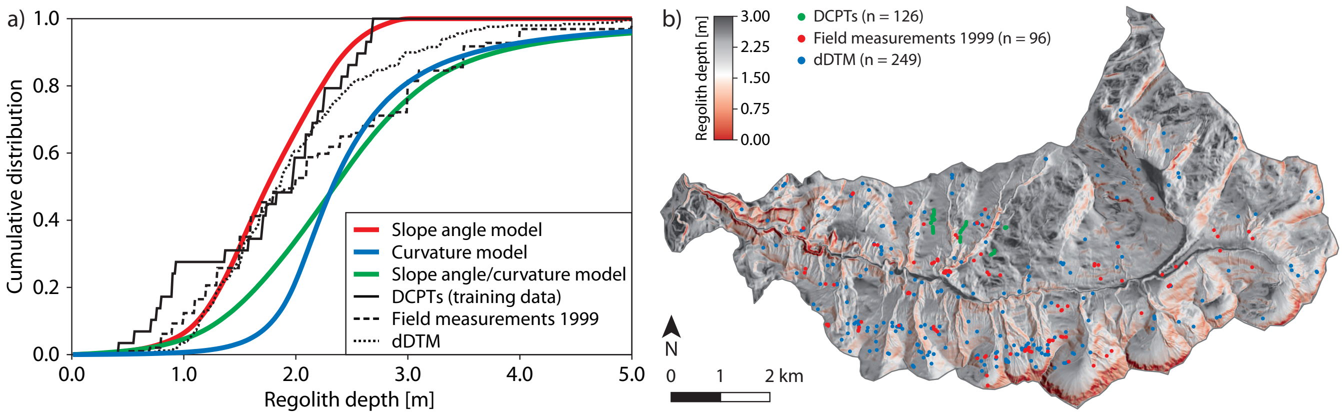

Figure 5. Cumulative distribution of d_{max} derived from observations and models (a) and the resulting regolith depth map (b).

to the closest settlements (BIN: Bingadels, BON: Bonacker, INN: Innerlaterns, MAZ: Mazona, REU: Reute, ROH: Rohnen). In the geological map (Fig. 2c) the sampled sites are mapped as hillslope debris (BIN-01, BIN-02), till deposits (INN, MAZ, ROH-01), Leimernmergel (BON) and Drusbergschichten (ROH-02). Back walls were laid open at the top of the landslide scarps. Two undisturbed and one disturbed sample were taken at two depths at each site except for location ROH-02. There, samples of one depth were considered sufficient because of the homogeneously structured regolith. The undisturbed samples were collected with the help of core cutters (diameter 9.6 cm) and stored airtight. Furthermore, buckets of material were taken from the respective depths. The grain size distributions (Fig. 6b), wet and dry bulk densities and water contents were determined for all samples. With the lower samples geotechnical parameters (φ', c', Atterberg limits) were derived from the respective laboratory tests (Fig. 6a,d). The upper samples were used to obtain estimates for the specific storage S_s based on the constrained modulus E_s [Pa] derived from oedometer tests (Rowe and Barden, 1966). The respective values for S_s [m^{-1}] were derived from

$$S_s = \rho_w \cdot g \cdot (\alpha_s + n \cdot \beta_w) \tag{5}$$

where ρ_w [kg m^{-3}] is the density of water, g is the acceleration of gravity (9.81 m s^{-2}), n is porosity, β_w is the compressibility of water (4.4×10^{-10} m^2 N^{-1}) and α_s [m^2 N^{-1}] is the compressibility of bulk soil, derived from

$$\alpha_s = \frac{3 \cdot (1-v)}{E_s \cdot (1+v)} \tag{6}$$

Table 2. Metadata for the eight sampled landslide sites and results of the conducted laboratory tests. *Results for a depth of 2.0 m.

Parameters	Unit	INN	MAZ	REU	BON	BIN-01	BIN-02	ROH-01	ROH-02
Latitude	Degree	47.2572	47.2679	47.2647	47.2673	47.2722	47.2737	47.2690	47.2699
Longitude	Degree	9.7381	9.7352	9.7144	9.7256	9.7040	9.7087	9.6980	9.7001
Sample depth 1	cm	56	37	34	30	45	42	41	-
Sample depth 2	cm	72	67	56	80	92	72	65	108
Eff. angle of internal friction	Degree	38.1	29.3	30.3	30.3	25.9	24.8	25.3	37.2
Effective cohesion	kPa	1.3	4.6	0.8	6.2	5.6	0.0	3.7	17.6
Constrained modulus*	kPa	1050	470	2040	240	1400	2740	400	750
Specific storage*	m^{-1}	0.037	0.031	0.007	0.061	0.011	0.005	0.037	0.020
Plastic limit	mass %	24.2	26.6	29.6	26.8	23.5	22.8	27.3	18.9
Liquid limit	mass %	31.1	41.8	49.1	46.2	40.0	47.1	47.9	23.1
Dry density	g cm^{-3}	1.43	1.45	1.27	1.37	1.36	1.84	1.25	1.99
Porosity	%	45.2	45.1	52.4	48.9	46.3	29.8	52.3	25.5
Soil type		Clay/silt	Silt	Silt	Clay	Clay	Clay	Clay	Clay/silt

where v is Poisson's ratio for which a constant value of $1/3$ was assumed (e.g. Lu and Godt, 2013; Schmidt et al., 2014). E_s depends on the prevailing stress level (i.e. overburden height; Schmidt et al., 2014) and was derived for a depth of 1–2 m (e.g. Berti and Simoni, 2010). The hydraulic diffusivity D_0 [m^2 s^{-1}] was derived from

$$D_0 = \frac{K_s}{S_s} \tag{7}$$

However, K_s was not tested in the field or laboratory. Its parameter values were calibrated over several orders of magnitude (Table 4). The background infiltration rate was set to zero in order to consider a conservative estimation of pore pressure conditions assuming a slope-parallel ground water flow (Baum et al., 2008, 2010).

For the parameters representing the effects of vegetation on slope stability in the revised model, spatially constant parameter values are assumed within the area covered by forest. A conservative set of parameter values is derived from respective literature with c_r set to 2.5 kPa (e.g. Bischetti et al., 2009; Steinacher et al., 2009), s_t set to 2.5 kPa (e.g. Steinacher et al., 2009) and d_r set to 1.0 m (e.g. Bischetti et al., 2009; Kutschera and Lichtenegger, 2002). However, these values were only applied within areas covered by forest. A forest cover map was prepared based on the normalized digital surface model (nDSM) derived from the ALS data from 2011. The areas covered by forest for the time of the two landslide-triggering rainfall events in August 2005 and May 1999 was adapted manually using high-resolution orthophotos from 2006 (ground sampling distance 0.125 m) and 2001 (ground sampling distance 0.25 m) respectively.

Nat. Hazards Earth Syst. Sci. Discuss., doi:10.5194/nhess-2017-73, 2017
Manuscript under review for journal Nat. Hazards Earth Syst. Sci.
Discussion started: 16 February 2017

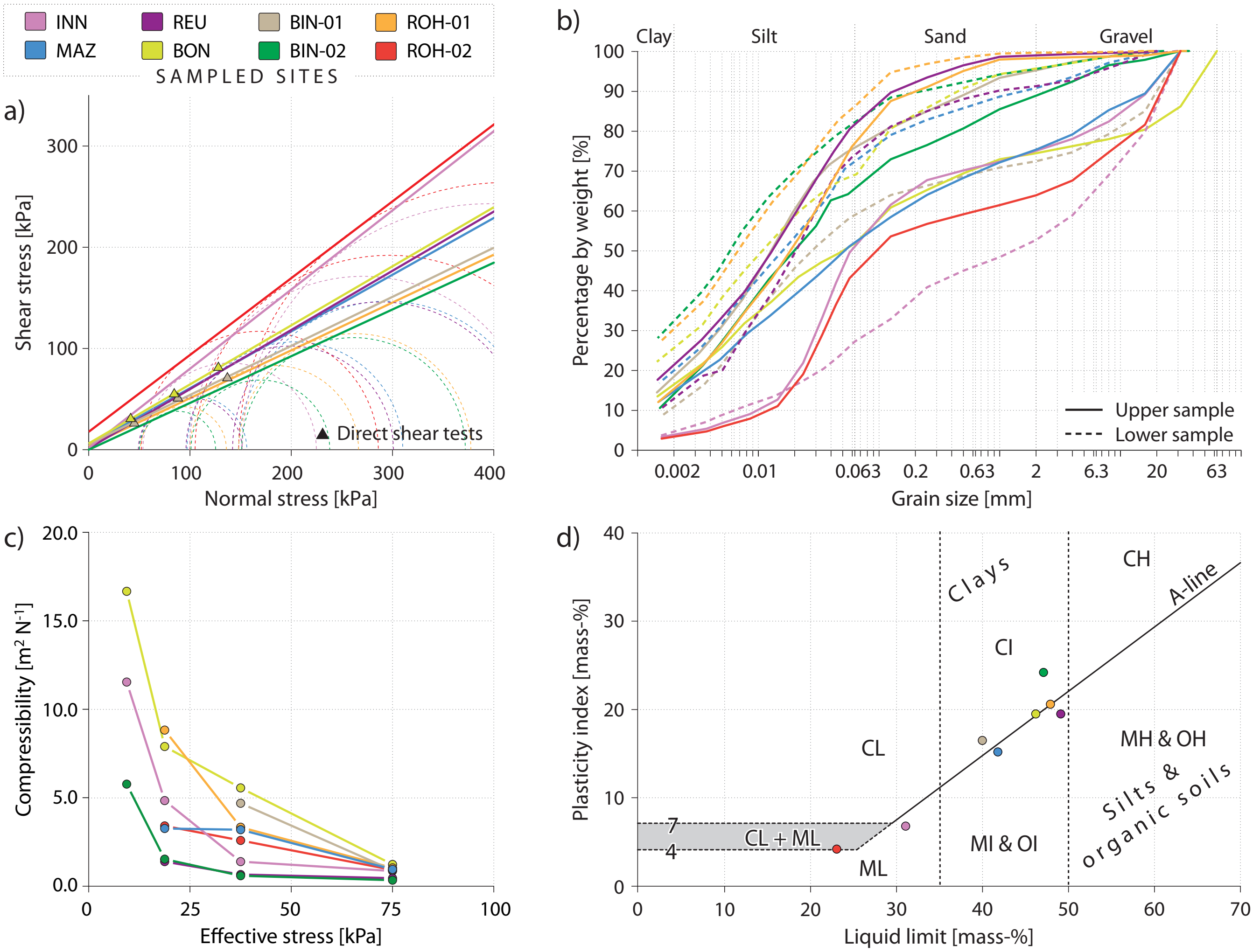

Figure 6. Results of the conducted laboratory tests. a) Direct and triaxial shear tests, b) grain size distributions, c) compressibility of bulk soil and d) Atterberg limits.

3.4 One-parameter-at-a-time sensitivity analysis

Following Hammond et al. (1992), the model's sensitivity against each parameter is tested individually (Fig. 8). For each parameter, central, minimum and maximum values are defined based on laboratory tests, field investigations and respective literature (Table 3). The resulting FOS_{p_i} for each parameter p_i sampled over the specified range is related to the respective $FOS_{p_{central}}$ based on the defined central parameter values:

$$\Delta FOS = \frac{FOS_{p_i} - FOS_{p_{central}}}{FOS_{p_{central}}} \tag{8}$$

Nat. Hazards Earth Syst. Sci. Discuss., doi:10.5194/nhess-2017-73, 2017
Manuscript under review for journal Nat. Hazards Earth Syst. Sci.
Discussion started: 16 February 2017

Natural Hazards and Earth System Sciences
Open Access
Discussions

Table 3. Parameter value ranges and central values considered in the OAT sensitivity analyses.

Parameter	Unit	Central value	Range	
			Minimum	Maximum
Eff. angle of internal friction	Degree	29.0	20.0	38.0
Cohesion (soil)	kPa	5.0	0.0	18.0
Root cohesion	kPa	2.5	0.0	5.0
Slope angle	Degree	30.0	20.0	40.0
Regolith depth	m	1.5	1.0	2.0
Unit weight of soil	kPa	18.5	17.0	20.0
Rooting depth	m	1.0	0.5	1.5
Tree surcharge	kPa	2.5	0.0	5.0
Specific storage	m^{-1}	0.010	0.001	0.100
Sat. hydraulic conductivity	$m\ s^{-1}$	10^{-6}	10^{-8}	10^{-4}
Depth of the water table	m	1.5	0.0	1.5
Precipitation (August 2005)	%	100	50	150

Table 4. Tested parameter values used for the calibration runs. For all 10,000 parameter value combinations time-dependent FOS-maps were computed for the landslide-triggering rainfall event in August 2005.

Parameter	Unit	1	2	3	4	5	6	7	8	9	10
Cohesion	kPa	0.0	2.0	4.0	6.0	8.0	10.0	12.0	14.0	16.0	18.0
Eff. angle of internal friction	deg	21.0	23.0	25.0	27.0	29.0	31.0	33.0	35.0	37.0	39.0
Sat. hydraulic conductivity	$m\ s^{-1}$	1.0×10^{-6}	2.2×10^{-6}	4.6×10^{-6}	1.0×10^{-5}	2.2×10^{-5}	4.6×10^{-5}	1.0×10^{-4}	2.2×10^{-4}	4.6×10^{-4}	1.0×10^{-3}
Specific storage	m^{-1}	1.0×10^{-3}	1.7×10^{-3}	2.8×10^{-3}	4.6×10^{-3}	7.7×10^{-3}	1.3×10^{-2}	2.2×10^{-2}	3.6×10^{-2}	6.0×10^{-2}	1.0×10^{-1}

The resulting relative deviation ΔFOS reflects the model's sensitivity against each parameter. However, interactions between parameters are not considered (Dobler and Pappenberger, 2013; Hammond et al., 1992).

3.5 Parameter calibration and validation

In previous studies, local OAT parameter tests are used for the calibration of parameter values (e.g. Gioia et al., 2016). In the present study, the calibration of the four identified sensitive parameters (φ', c', K_s, S_s; Sect. 4.1) is based on systematic testing of parameter value combinations for the whole catchment (global calibration), computed with a HPCC (162 nodes, 1.944 Intel Xeon Gulftown compute cores). For each parameter, ten values are sampled from a uniform distribution in equal increments from the defined minimum to maximum (e.g. Beven and Freer, 2001). Because of the limited number of laboratory tests it is not possible to infer a probability distribution of the parameter values. The hydrological parameters are sampled on the logarithmic scale (Table 4).

Nat. Hazards Earth Syst. Sci. Discuss., doi:10.5194/nhess-2017-73, 2017
Manuscript under review for journal Nat. Hazards Earth Syst. Sci.
Discussion started: 16 February 2017

Natural Hazards and Earth System Sciences
Discussions

The predictive performance of each FOS map resulting from the 10,000 calibration runs with seven time steps each (514.9 gigabyte of data), was assessed with the receiver operating characteristic (ROC) principle (Begueria, 2006). Using physically-based slope stability models, a $FOS < 1$ indicates a potential slope failure, while a $FOS \geq 1$ suggests a stable slope. The coordinates of the point in the ROC-plot where the FOS falls below 1.0 represent the correctly predicted observed landslides (true positives; TP) and non-landslides (true negatives; TN). The basic idea of the calibration procedure is to identify parameter value combinations, which result in an optimal prediction of observed landslides and non-landslides (Fig. 7). Data processing and analysing included the open source GRASS GIS 6.4 (GRASS Development Team, 2014), Python 2.7 programming language (Python Software Foundation, 2016) and R statistical software (R Core Team, 2016).

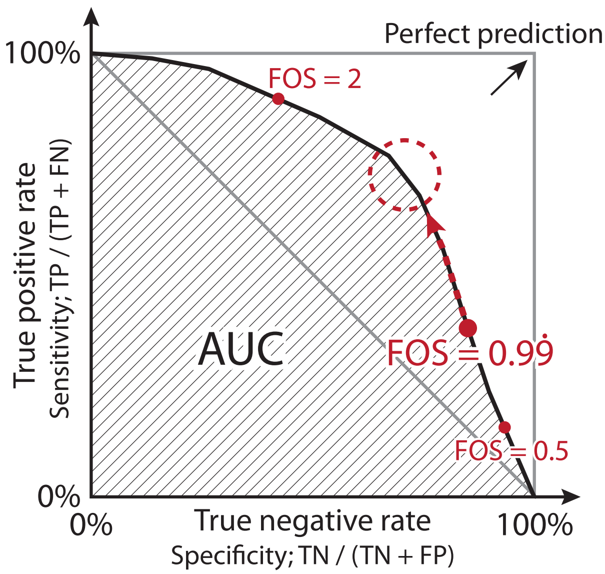

Figure 7. Principle of the calibration procedure. FOS: factor of safety, TP: true positives, FN: false negatives, TN: true negatives, FP: false positives, AUC: area under the ROC-curve.

The identification of 'behavioural model runs' out of the 10,000 calibration runs is based on the following observations and assumptions:

1. At the beginning of the simulations the slopes throughout the Laternser valley must be stable ($FOS \geq 1.0$).
2. Most shallow landslides were triggered after the highest precipitation intensity occurred (FOS falls below 1.0).
3. Optimal parameter values can be derived from the simulations that correctly predict the most landslides while satisfying the first two assumptions.

The necessary observations for the assessment of the predictive performance are obtained from the shallow landslide inventory. For 261 out of 356 shallow landslides triggered in August 2005 the scar areas are available, delineated with the help of a dDTM (Zieher et al., 2016). A shallow landslide is regarded as correctly predicted, if the FOS falls below 1.0 in at least

Nat. Hazards Earth Syst. Sci. Discuss., doi:10.5194/nhess-2017-73, 2017
Manuscript under review for journal Nat. Hazards Earth Syst. Sci.
Discussion started: 16 February 2017

one raster cell intersecting the scar area. For landslides with no scar area mapped (95 landslides triggered in August 2005, landslides triggered in May 1999), a planimetric circle with a diameter of 5.6 m (resulting in an area of 100 m^2) around the scar point (mapped in the visual center of the scar areas) is used instead.

4 Results

4.1 One-parameter-at-a-time sensitivity analysis

The OAT sensitivity analysis of the geomechanical model element's parameters reveals that an increase in parameter values can have positive (φ', c' and c_r) and negative effects (β, d_{max}, s_t) on slope stability (Fig. 8a). Variations in β and d_{max} result in non-linear effects on slope stability. An increase in β or d_{max} lowers the FOS. Both parameters are derived from a DTM and direct field measurements. Increased parameter values for φ' and c' distinctively enhance the FOS. Their impact is greater than the effects of the parameters associated with the vegetation (c_r, s_t, d_r). While variations of s_t have minor destabilizing effects, modified values of c_r increase the FOS. For the tested parameterization, variations of d_r do not show effects on the FOS. In the calibration procedure, the parameters representing the effects of vegetation are kept constant within the respective areas covered by forest while the parameters φ' and c' are tested systematically.

For the parameters of the hydrological model element the sensitivity analysis is based on the precipitation time series from 22/23 August 2005 to account for time-dependent responses. The model's sensitivity against the precipitation input is tested with scaled time series of this rainfall event. Depending on the previous precipitation input, the parameters K_s, S_s and d_{wi} have different effects on the resulting FOS. Reducing K_s by two orders of magnitude, the FOS increases up to 30% due to the lowered infiltration while higher parameter values result in a reduced FOS as reaction to the enhanced infiltration. The magnitude of S_s essentially controls the temporal dynamics of the modelled infiltration process. By reducing S_s, the value of D_0 increases (Eq. 7), leading to a quicker infiltration of the precipitation input. Thus, lowering the S_s by one order of magnitude leads to a reduction of the FOS by more than 20% while higher parameter values lead to an enhanced FOS. Decreasing the d_{wi} by 100% (initial water table at the surface) results in a reduced FOS by 24%. Compared to the other hydrological parameters, the model's sensitivity against the scaled precipitation time series is lower. By varying the precipitation input within a range of ±50%, the resulting FOS changes by -4% to +9%. The precipitation input is given by the interpolated hourly precipitation sums and the d_{wi} is set to the regolith/bedrock interface for the calibration procedure with the rainfall event in August 2005 while the parameters K_s and S_s are tested systematically.

4.2 Calibration with the landslide-triggering rainfall event in August 2005

The temporal prediction rates and the respective coordinates for $FOS = 0.9\dot{9}$ in the ROC-curve for the shallow landslides triggered on 22/23 August 2005 are shown in Fig. 9. Table 5 shows the respective minimum and maximum prediction rates for the calibration steps. The area under the ROC-curve (AUC) as a measure of the overall predictive performance (Begueria, 2006) is based on the full FOS range of the resulting maps. Considering all 10,000 calibration runs (Fig. 9a), many parameter

Nat. Hazards Earth Syst. Sci. Discuss., doi:10.5194/nhess-2017-73, 2017
Manuscript under review for journal Nat. Hazards Earth Syst. Sci.
Discussion started: 16 February 2017

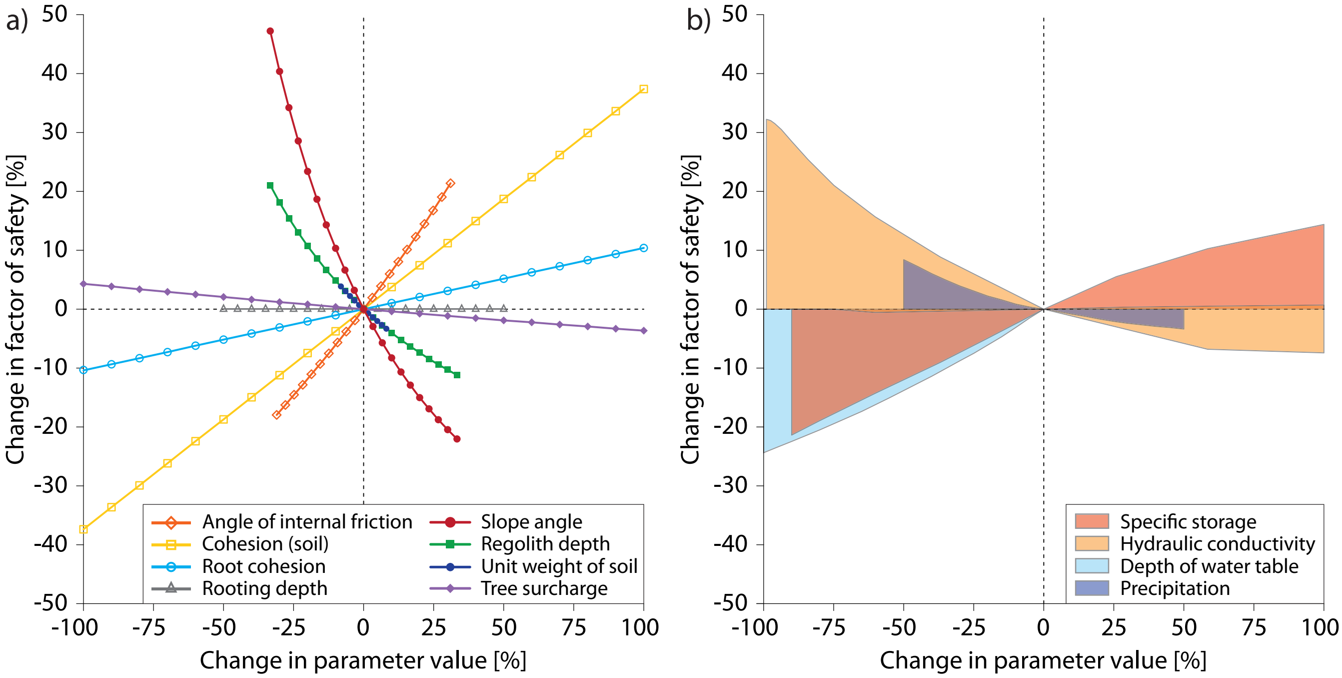

Figure 8. OAT sensitivity of the model results (change in factor of safety) for tested parameter value ranges for the geomechanical model element (a) and the hydrological model element (b). Respective parameter values are listed in Table 3.

combinations yield completely stable conditions over all computed time steps (no correctly predicted landslides; $TPR = 0.0\%$) but also too unstable conditions at time step $t = 0$. Allowing for 0.5% of the catchment area to fail at time step $t = 0$, 7,300 calibration runs remain (Fig. 9b). However, many of the remaining calibration runs predict slope failures before the onset of the landslide-triggering rainfall event. Assuming that most shallow landslides were triggered after the maximum precipitation intensity, 1,134 calibration runs remain (Fig. 9c). Several of these remaining calibration runs do not predict any of the observed shallow landslides ($TPR = 0.0\%$). Therefore the 25 calibration runs with the highest sum of correctly predicted landslides and non-landslides are selected ('behavioural model runs', Fig. 9d). With these model runs, the location and the supposed triggering timing of 46.6 to 70.5% of the observed shallow landslides can be predicted while 71.0 to 90.3% of the observed non-landslides remain stable. It is assumed that this identified model ensemble is able to represent the spatial and temporal occurrence of shallow landslides triggered on 22/23 August 2005. The resulting parameter value combinations are regarded optimal for the dynamic modelling slope stability in the Laternser valley.

4.3 Validation with the landslide-triggering rainfall event in May 1999

To test the identified model ensemble's predictive performance, it is applied for the landslide-triggering rainfall event in May 1999. Despite the different nature of the rainfall events (August 2005: short and intense; May 1999: prolonged and less intense), most landslides are again predicted after the highest precipitation intensity (time step 6; after 45h; Fig. 10). Hence, assuming

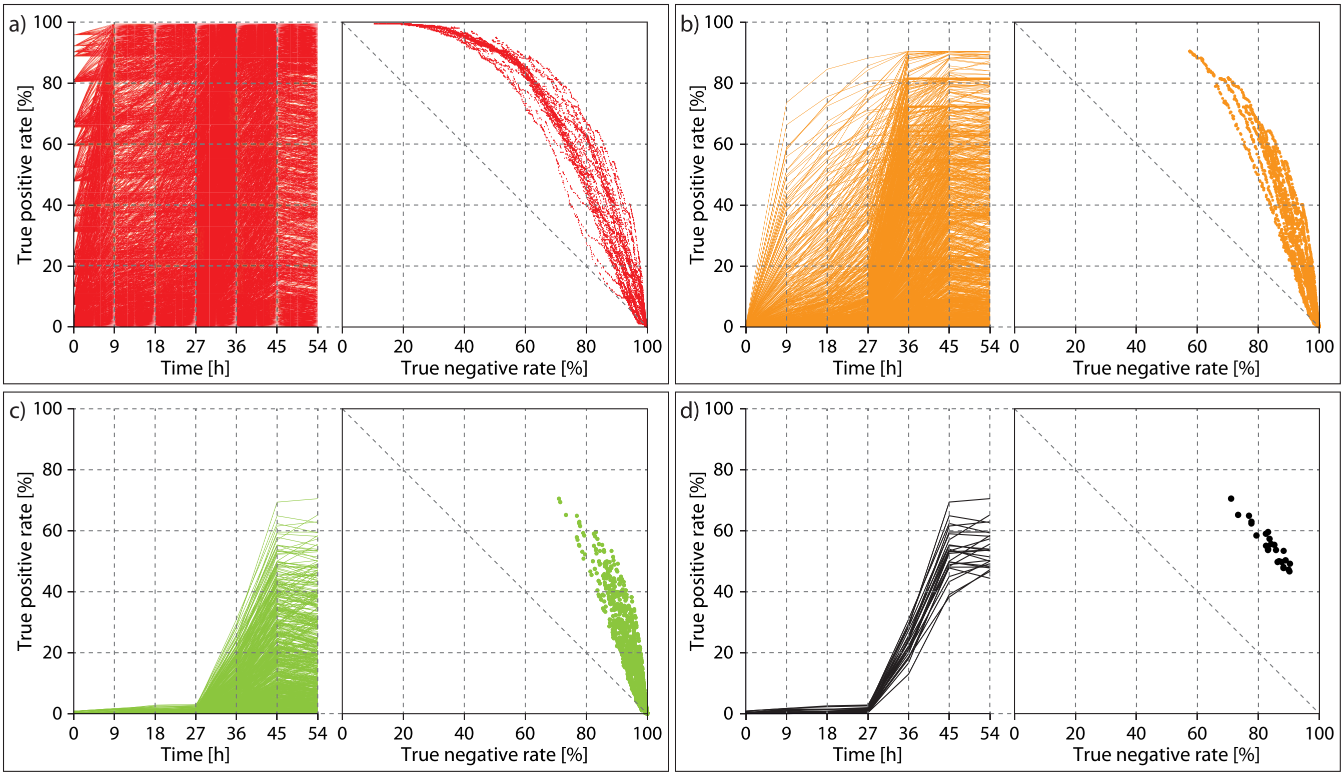

Figure 9. Temporal prediction rate for the seven time steps and rate of correctly predicted landslides (true positives) and non-landslides (true negatives) at $FOS = 0.9\dot{9}$ for the calibration runs. All 10,000 calibration runs (a), calibration runs which satisfy assumption 1 (b; n = 7,300), calibration runs which satisfy assumption 2 (c; n = 1,134) and the 25 calibration runs which predict most landslides and non-landslides (d). In d, only the coordinates of the highest true positive rate for the 25 calibration runs are shown.

Table 5. Prediction rates of the model ensemble for the landslide-triggering rainfall event in August 2005. TPR: true positive rate, TNR: true negative rate, FPR: false positive rate, FNR: false negative rate, AUC: area under the ROC-curve.

Prediction	All calibration runs		Stable at t = 0		Most landslides at t = 45		Best 25 runs	
	Minimum	Maximum	Minimum	Maximum	Minimum	Maximum	Minimum	Maximum
TPR	0.0%	99.4%	0.0%	90.4%	0.0%	70.5%	46.6%	70.5%
FNR	0.6%	100.0%	9.6%	100.0%	29.5%	100.0%	29.5%	53.4%
TNR	10.6%	100.0%	57.5%	100.0%	71.0%	100.0%	71.0%	90.3%
FPR	0.0%	89.4%	0.0%	42.5%	0.0%	29.0%	9.7%	29.0%
AUC	71.8%	84.3%	73.1%	84.3%	73.1%	84.0%	78.1%	83.5%

that the landslides observed for the rainfall event on 21/22 May 1999 were triggered after the maximum precipitation intensity occurred, the model ensemble is able to predict the location and the supposed triggering timing of most of these landslides.

Table 6. Prediction rates of the model ensemble for the landslide-triggering rainfall event in May 1999. Three scenarios for the initial depth of the ground water table in relation to regolith depth are considered. TPR: true positive rate, TNR: true negative rate, FPR: false positive rate, FNR: false negative rate, AUC: area under the ROC-curve.

Description	Regolith depth		0.75×regolith depth		0.50×regolith depth	
	Minimum	Maximum	Minimum	Maximum	Minimum	Maximum
TPR	43.9%	79.3%	51.2%	89.0%	58.5%	95.1%
FNR	20.7%	56.1%	11.0%	48.8%	4.9%	41.5%
TNR	71.5%	91.5%	66.1%	89.1%	62.7%	88.6%
FPR	8.5%	28.5%	10.9%	33.9%	11.4%	37.3%
AUC	82.3%	87.6%	84.1%	87.8%	85.2%	87.2%

However, the melting of the accumulated snow from the preceding winter may have lead to an enhanced soil moisture and a rise of the water table. Therefore, three scenarios for the d_{wi} were considered (100%, 75% and 50% of the regolith depth; Fig. 10, Table 6). Assuming the d_{wi} to be at the regolith/bedrock interface, between 43.9–79.3% of the observed landslides are predicted correctly. Increasing the d_{wi} to 75% of the regolith depth, the true positive rate rises to 51.2–89.0% with up to 4.9% of the landslides predicted at $t = 0$. By further increasing the d_{wi} to 50% of the regolith depth, the true positive rate rises to 58.5–95.1% while up to 30.3% of the landslides predicted at $t = 0$. Setting d_{wi} to 75% of the regolith depth is therefore considered adequate for simulating slope stability for the landslide-triggering rainfall event in May 1999.

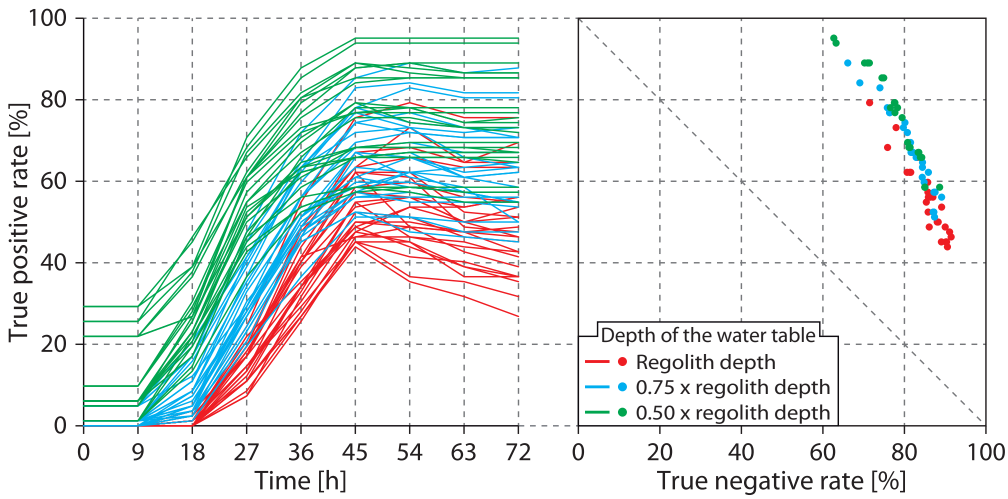

Figure 10. Temporal prediction rate (a) and coordinates for $FOS = 0.9\dot{9}$ based on the model ensemble for the landslide-triggering rainfall event in May 1999. Three scenarios for the initial conditions (initial depth of the water table) are considered.

Table 7. Prediction rates of the model ensemble for the landslide-triggering rainfall events in May 1999 and August 2005. For the rainfall event in May 1999 an initial depth of the water table of $0.75\times$regolith depth was considered. TPR: true positive rate, TNR: true negative rate, FPR: false positive rate, FNR: false negative rate, AUC: area under the ROC-curve.

Description	May 1999		August 2005	
	Minimum	Maximum	Minimum	Maximum
TPR	51.2%	89.0%	46.6%	70.5%
FNR	11.0%	48.8%	29.5%	53.4%
TNR	66.1%	89.1%	71.0%	90.3%
FPR	10.9%	33.9%	9.7%	29.0%
AUC	84.1%	87.8%	78.1%	83.5%

4.4 Comparison of the model ensemble's predictive performance

Figure 11 shows the resulting areas of slope failures predicted by the model ensemble for both rainfall events. The colors indicate the number of model runs predicting slope failures per raster cell. Areas shown in red indicate a high agreement of the model ensemble while yellow areas are identified by only one model run. The coordinates in the ROC plots associated with the number of agreeing model runs are shown in Fig. 11c for the rainfall event in August 2005 and Fig. 11f for the rainfall event in May 1999. The single model run which predicts most landslides correctly also entails the lowest TNR of the model ensemble. With all 25 model runs in agreement the rate of correctly predicted landslides is distinctively lower while the TNR increases markedly. The prediction rates of the 25 model runs are shown in Fig. 11d for the rainfall event in August 2005 and Fig. 11e for the rainfall event in May 1999. Respective maximum and minimum prediction rates are listed in Table 7. Generally, the model ensemble better predicts the landslides triggered in May 1999. However, non-landslides are better predicted for the rainfall event from August 2005.

In total, the model ensemble correctly predicts 73.0% of the landslides triggered in August 2005 (landslides, which are predicted correctly by at least on ensemble model run). This is slightly more than the best single model run of the ensemble. Apparently, some observed landslides which cannot be explained by the best single model run (TPR 70.5%) are explained by other model runs. Landslides observed on open land are predicted better (206 out of 268; 76.9% correctly predicted) than in the forest (54 out of 88; 61.4%). For the landslide-triggering rainfall event in May 1999, 91.5% of the observed landslides are predicted correctly. Like for the results for the rainfall event in August 2005, some additional landslides are explained by the model ensemble compared to the best single model run (TPR 89.0%). On open land, landslides are again predicted better (51 out of 54; 94.4% correctly predicted) than in the forest (24 out of 28; 85.7%).

4.5 Calibrated parameter values

Unlike the OAT sensitivity analysis, the presented calibration procedure can reveal parameter interactions. The calibrated parameter values are shown in (Fig. 12). For the geotechnical parameters, ranges of 21°–35° for the angle of internal friction

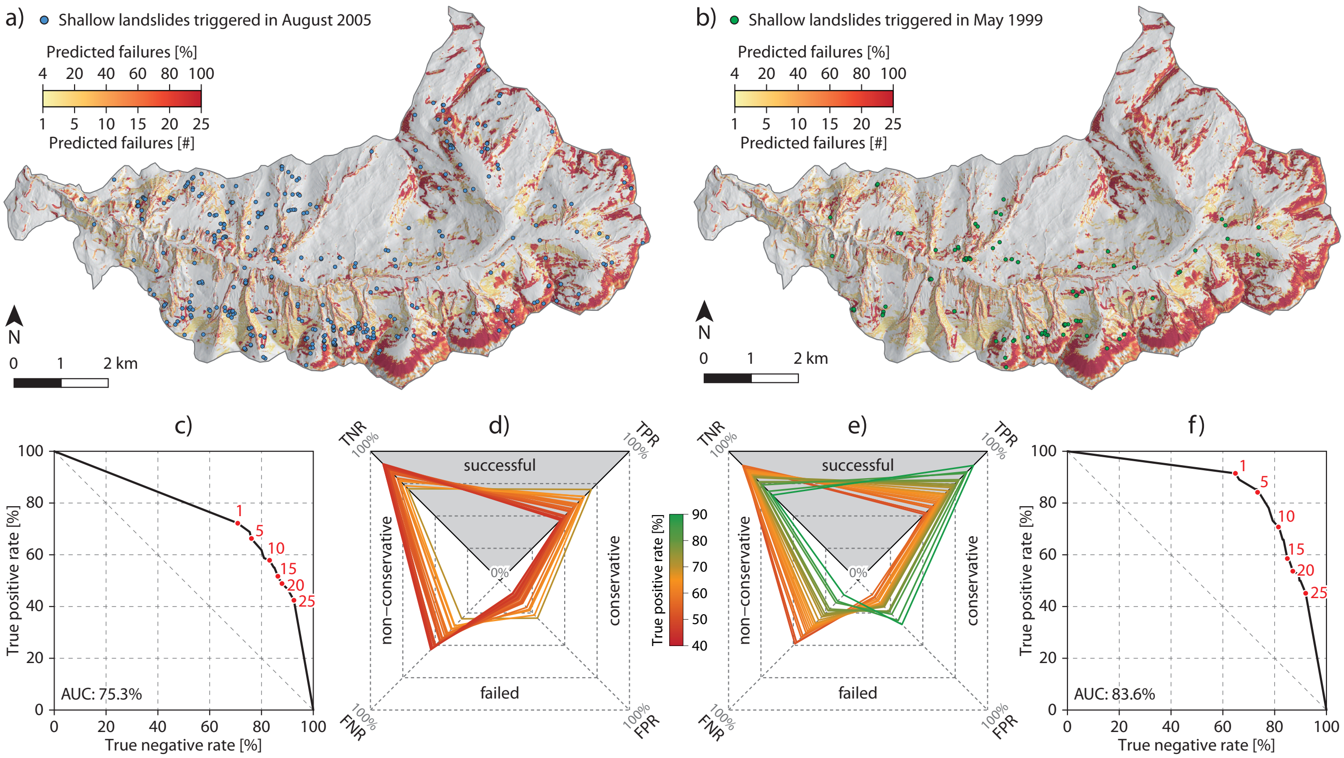

Figure 11. Predictive performance of the model ensemble. The maps show areas predicted to fail in response to the rainfall event in August 2005 (a) and in May 1999 (b). The colors indicate the number of models predicting the respective areas to fail. The ROC plots likewise show the coordinates of the correctly predicted landslides and non-landslides for August 2005 (c) and May 1999 (f) associated with the number of models which are in agreement. The predictive rates of the model ensemble (see Table 7) are visualized for August 2005 (d) and May 1999 (e). The colors indicate the true positive rate. TPR: true positive rate, TNR: true negative rate, FPR: false positive rate, FNR: false negative rate, AUC: area under the ROC-curve.

and 4–8 kPa for the cohesion are optimal value ranges. Furthermore, the distribution of the calibrated geotechnical parameters suggest, that lower angles of internal friction can be compensated by increasing the cohesion and vice versa. In case of the hydrological parameters, the calibration procedure reveals optimal value ranges between 10^{-6}–10^{-5} m s^{-1} for the hydraulic conductivity and 10^{-2}–10^{-1} m^{-1} for the specific storage. The resulting hydraulic diffusivity (Eq. 7) is in the range of 10^{-5}–10^{-3} m^{2} s^{-1}. These ranges theoretically cover a variety of materials from sands to clays (e.g. Prinz and Strauß, 2011).

4.6 Model ensemble's sensitivity against increased precipitation intensity

According to the Austrian Assessment Report (Kromp-Kolb et al., 2014), frequency and magnitude of extreme precipitation events are expected to increase over Austria in a future climate. Using the model ensemble, the impact of increasing precipitation intensity on shallow landslide susceptibility is assessed. Therefore, the precipitation input from August 2005 is scaled

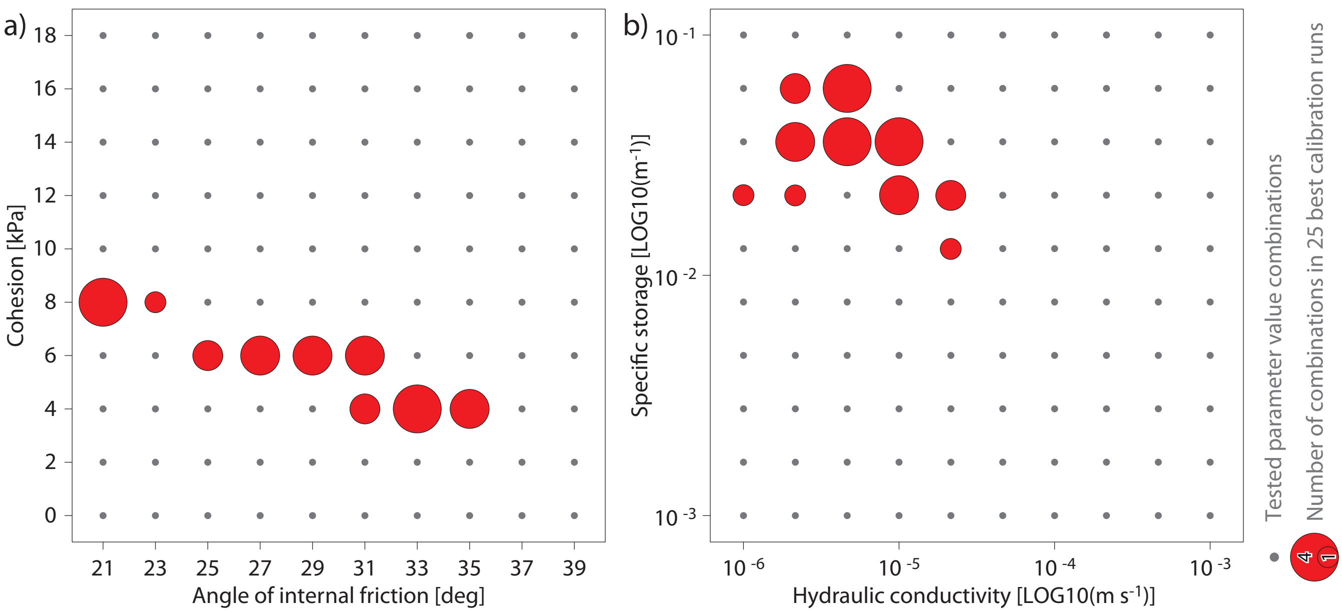

Figure 12. Calibrated values for the geotechnical (a) and hydrological parameters (b). The sizes of the red circles indicate the number of model runs based on these value pairs (with varying values of the further tested parameters).

up to 125% in increments of 5% (Fig. 13a). The resulting change in the proportion of unstable areas is shown in Fig. 13b. It increases from 7.6% (±2.4%; 1 standard deviation) for the original rainfall event in August 2005 to 8.5% (±2.7%) for the same rainfall event scaled to 125%.

At the same time, the predicted mean surface runoff observed at time step 40h (time step with the highest runoff) increases distinctively. It rises from 9.8×10^{-4} m s^{-1} ($\pm 1.3 \times 10^{-3}$ m s^{-1}; 1 standard deviation) for the original rainfall event in August 2005 to 1.7×10^{-3} m s^{-1} ($\pm 1.8 \times 10^{-3}$ m s^{-1}) for the same rainfall event scaled to 125%. This is an increase of 76.0% compared to the runoff generated with the original rainfall input from August 2005 (Fig. 13c).

5 Discussion

The OAT sensitivity analysis reveals a high impact of the slope angle and the regolith depth on the resulting FOS. The slope angle map is derived area-wide from a DTM based on ALS data. Their accuracy is considered sufficient for the derivation of slope angles at a spatial resolution of 10 m. However, resulting slope angles may differ depending on the respective calculation method (e.g. Horn, 1981; Wood, 1996). The regolith depth map used in this study is based on a linear model with the slope angle as the only predictor. It is shown that this model is suitable to predict the cumulative distribution of regolith depth for depths up to 2.0 m. However, its spatial distribution may be better reproduced with techniques including more predictors (e.g. Catani et al., 2010; Tesfa et al., 2009). Compared to the impact of the geotechnical parameters, the effect of the vegetation are considerably small. However, this can be attributed to the conservative set of parameter values.

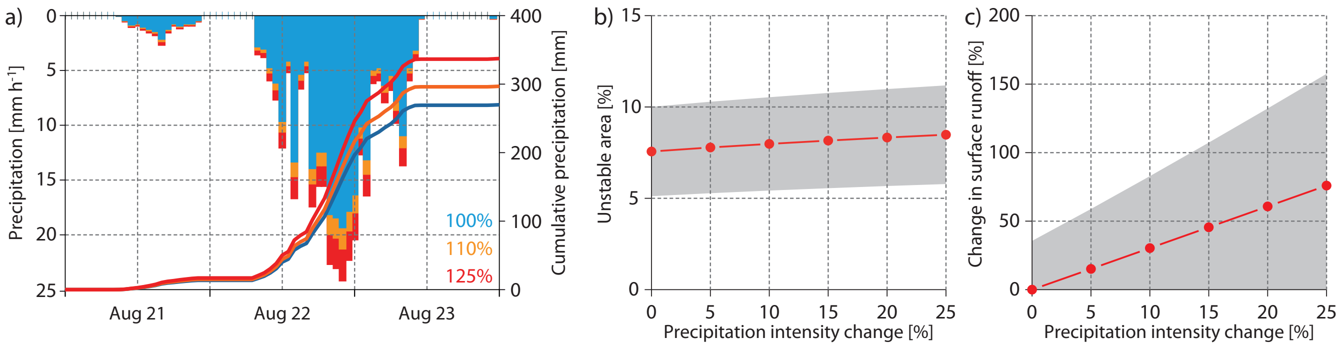

Figure 13. Scaled rainfall event of August 2005 (a) and resulting changes in slope stability based on the ensemble runs with a scaled precipitation input (b). The area shaded in grey shows one standard deviation.

For the calibration procedure, the tested parameters are assumed to be constant throughout the catchment area. In other studies, property zones according to the geological substratum are defined with varying parameter value ranges. However, for the proposed calibration procedure interactions between such property zones would have to be included (e.g. enhanced runoff from zones above with lower infiltration capacity). Considering such interactions would exceed the available computational capabilities.

In the calibration procedure, FOS maps were calculated for seven time steps with intervals of nine hours. Due to computational reasons it was not possible to compute hourly output maps. Therefore, the model's predictive performance between these time steps remains unknown. It is possible that the model is able to predict more landslides correctly, if more time steps could be considered. As shown for both landslide-triggering rainfall events, some of the ensemble model runs show a decrease in the temporal true positive rate after the maximum precipitation intensity. This observation is associated with decreasing pore pressures due to less infiltrating water. For some observed landslides which are predicted to fail around the maximum precipitation intensity, the reduced pore pressure afterwards causes the FOS to rise above 1 and hence predicts stable slopes again. However, this behaviour also suggests a sufficient calibration of the parameter values. In the same sense, parameter values were tested in discrete intervals. The application of parameter values in between also could increase the models predictive performance. Hence, the assessed predictive performance must be considered as a conservative estimate.

With the model runs of the identified model ensemble between 46.6–70.5% of the observed landslides triggered in August 2005 and 51.2–89.0% of the observed landslides triggered in May 1999 can be predicted correctly. In total, the model ensemble correctly predicts 73.0% of the landslides triggered in August 2005 and 91.5% of the observed landslides triggered in May 1999. A direct comparison with prediction rates of further studies conducted in other study areas is difficult since site-specific characteristics (e.g. soil material, conditions prior to landslide triggering, size of the study area) and data availability and quality (e.g. landslide inventory, DTM) may vary considerably. Still, the model ensemble fails to predict the remaining 27.0% of the landslides triggered in August 2005 and 8.5% of the landslides triggered in May 1999. Furthermore, the identified model ensemble cannot explain why landslides triggered in August 2005 were not triggered in May 1999. Areas predicted as unstable are in good agreement for both rainfall events. Further local factors may control the triggering of the landslides (e.g. local precipitation patterns, preferential flow, concentrated surface runoff, locally weak layers). Such local effects and properties are not covered by the model nor the input parameter maps. Moreover, the geomechanical model element includes a simplified representation of landslide geometry while an instant failure mechanism of the whole landslide is assumed. The model's simplifications of complex processes together with the applied parametrization may explain the shortfall in spatial and temporal prediction accuracy.

The results of the identified model ensemble suggest a lower prediction rate of shallow landslides located in the forest. Therefore, the chosen representation of the effects of vegetation on slope stability in revised model may be too simple. Furthermore, a conservative, spatially constant set of parameter values was chosen for the parameters describing the effects of vegetation. In forest stands, these parameter values vary spatially according to tree species, age and density. Parameter maps for the effects of vegetation accounting for these attributes could further improve the model's predictive performance (e.g. Schwarz et al., 2010, 2012).

The results of the model ensemble based on a scaled precipitation intensity suggest a slight positive trend of unstable areas while the surface runoff increases markedly. However, since subsurface flow is not considered and the runoff is calculated for each time step individually, the model will fail in predicting actual stream flow. Nevertheless, this result suggests that the precipitation intensities during landslide-triggering rainfall events are already close to or above the infiltration capacity under present-day conditions. A potential increase in precipitation intensity might thus lead to an increase in surface runoff rather than slope failure. However, considering the uncertainty indicated by the model ensemble, both trends are not significant.

6 Conclusions

In the present study, a revised form of the model TRIGRS 2.0 is calibrated based on a limited number of laboratory tests and a detailed shallow landslide inventory. The parameter space of four identified sensitive parameters is tested systematically. A model ensemble including 25 'behavioural model runs' is identified which correctly predicts the most landslides and non-landslides for a landslide-triggering rainfall event in August 2005. The predictive performance of this ensemble is tested for a landslide-triggering rainfall event in May 1999. Finally, the ensemble is used to quantify potential changes in slope stability associated with increasing rainfall intensities.

It is shown that despite the simplified representation of the involved processes the location and the supposed triggering timing of 73.0% of the observed landslides triggered in August 2005 and 91.5% of the observed landslides triggered in May 1999 are predicted correctly by the identified model ensemble. The inability of the model to correctly predict the remaining landslides may be in part related to the simplifications of the related processes. To overcome these issues, additional processes should be included in the model (e.g. subsurface flow). However, an unresolved issue remains the spatial variability of the input parameter values.

The assessment of changes in slope stability associated with scaled precipitation input shows a slight increase in potentially affected areas. At the same time, the peak runoff increases markedly. Despite both trends are not significant, this could indicate that the precipitation intensities of past landslide-triggering rainfall events were already close to the soil's infiltration capacity. However, a general increase in precipitation intensity could lead to an increase in the frequency of landslide-triggering rainfall events. Rainfall events which did not trigger any shallow landslides in the past may become trigger events under a changing climate in future.

Acknowledgements. We thank the federal state of Vorarlberg and the Hydrographic Service of Vorarlberg (HD) for kindly providing data for this study. The computational results presented have been achieved (in part) using the HPC infrastructure LEO of the University of Innsbruck. This work has been conducted within the project C3S-ISLS, which is funded by the Austrian Climate and Energy Fund, 5th ACRP Program.

References

Amann, G., Schennach, R., Kessler, J., Maier, B., and Terzer, S.: Handbuch der Vorarlberger Waldgesellschaften, vol. 2, Amt der Vorarlberger Landesregierung, Abteilung Forstwesen, 2014.

Andrecs, P., Markart, G., Lang, E., Hagen, K., Kohl, B., and Bauer, W.: Untersuchung der Rutschungsprozesse vom Mai 1999 im Laternsertal (Vorarlberg), BFW Berichte, 127, 55–87, 2002.

Bathurst, J. C., Moretti, G., El-Hames, A., Moaven-Hashemi, A., Burton, A., et al.: Scenario modelling of basin-scale, shallow landslide sediment yield, Valsassina, Italian Southern Alps, Natural Hazards and Earth System Science, 5, 189–202, doi:10.5194/nhess-5-189-2005, http://dx.doi.org/10.5194/nhess-5-189-2005, 2005.

Baum, R. L., Savage, W. Z., and Godt, J. W.: TRIGRS- A Fortran Program for Transient Rainfall Infiltration and Grid-Based Regional Slope-Stability Analysis, Version 2. 0, Tech. rep., U. S. Geological Survey, 2008.

Baum, R. L., Godt, J. W., and Sacage, W. Z.: Estimating the timing and location of shallow rainfall-induced landslides using a model for transient, unsaturated infiltration, Journal of Geophysical Research, 115, F03 013, doi:10.1029/2009JF001321, http://dx.doi.org/10.1029/2009JF001321, 2010.

Begueria, S.: Validation and Evaluation of Predictive Models in Hazard Assessment and Risk Management, Natural Hazards, 37, 315–329, doi:10.1007/s11069-005-5182-6, http://dx.doi.org/10.1007/s11069-005-5182-6, 2006.

Berti, M. and Simoni, A.: Field evidence of pore pressure diffusion in clayey soils prone to landsliding, Journal of Geophysical Research: Earth Surface, 115, 1–20, doi:10.1029/2009JF001463, http://dx.doi.org/10.1029/2009JF001463, 2010.

Beven, K. and Freer, J.: Equifinality, data assimilation, and uncertainty estimation in mechanistic modelling of complex environmental systems using the GLUE methodology, Journal of Hydrology, 249, 11–29, doi:10.1016/S0022-1694(01)00421-8, http://dx.doi.org/10.1016/S0022-1694(01)00421-8, 2001.

Beven, K. and Kirkby, M.: A physically based, variable contributing area model of basin hydrology, Hydrol. Sci. Bull., 24, 43–69, doi:10.1080/02626667909491834, http://dx.doi.org/10.1080/02626667909491834, 1979.

Bischetti, G., Chiaradia, E., Epis, T., and Morlotti, E.: Root cohesion of forest species in the Italian Alps, Plant and Soil, 324, 71–89, doi:10.1007/s11104-009-9941-0, http://dx.doi.org/10.1007/s11104-009-9941-0, 2009.

Bischetti, G. B., Chiaradia, E. A., Simonato, T., Speziali, B., Vitali, B., Vullo, P., and Zocco, A.: Root strength and root area ratio of forest species in Lombardy (Northern Italy), Plant and Soil, 278, 11–22, doi:10.1007/s11104-005-0605-4, http://dx.doi.org/10.1007/s11104-005-0605-4, 2005.

Bollinger, D., Hegg, C., Keusen, H., and Lateltin, O.: Ursachenanalyse der Hanginstabilitäten 1999. Arbeitsgruppe Geologie und Naturgefahren (AGN) Teil A: Allgemeiner Teil: Aspekte der Hangstabilität, in: Bulletin für angewandte Geologie, vol. 5/1, pp. 5–38, AGN, 2000.

Carrara, A., Cardinali, M., Detti, R., Guzzetti, F., Pasqui, V., and Reichenbach, P.: GIS techniques and statistical models in evaluating landslide hazard, Earth Surf. Process. Landforms, 16, 427–445, doi:10.1002/esp.3290160505, http://dx.doi.org/10.1002/esp.3290160505, 1991.

Catani, F., Segoni, S., and Falorni, G.: An empirical geomorphology-based approach to the spatial prediction of soil thickness at catchment scale, Water Resources Research, 46, W05 508, doi:10.1029/2008WR007450, http://dx.doi.org/10.1029/2008WR007450, 2010.

Crosta, G. B. and Frattini, P.: Distributed modelling of shallow landslides triggered by intense rainfall, Natural Hazards and Earth System Science, 3, 81–93, doi:10.5194/nhess-3-81-2003, http://dx.doi.org/10.5194/nhess-3-81-2003, 2003.

Cruden, D. M. and Varnes, D. J.: Landslides: Investigation and Mitigation, vol. 247, chap. Landslide types and processes, pp. 36–75, National Academies Press, 1996.

Davis, J. L. and Annan, A. P.: Ground-penetrating radar for high-resolution mapping of soil and rock stratigraphy, Geophysical Prospecting, 37, 531–551, doi:10.1111/j.1365-2478.1989.tb02221.x, http://dx.doi.org/10.1111/j.1365-2478.1989.tb02221.x, 1989.

Dietrich, W. and Montgomery, D.: Shalstab: a digital terrain model for mapping shallow landslide potential. [WWW document, accessed May 2015], http://socrates.berkeley.edu/~geomorph/shalstab/, 1998.

Dietrich, W. E., Reiss, R., Hsu, M.-L., and Montgomery, D. R.: A process-based model for colluvial soil depth and shallow landsliding using digital elevation data, Hydrological Processes, 9, 383–400, doi:10.1002/hyp.3360090311, http://dx.doi.org/10.1002/hyp.3360090311, 1995.

Dobler, C. and Pappenberger, F.: Global sensitivity analyses for a complex hydrological model applied in an Alpine watershed, Hydrological Processes, 27, 3922–3940, doi:10.1002/hyp.9520, http://dx.doi.org/10.1002/hyp.9520, 2013.

Fairbridge, R. W.: The Encyclopedia of Geomorphology. Encyclopedia of Earth Sciences Series, vol. 3, Dowden, Hutchinson & Ross Stroudsburg, Pennsylvania, 1968.

Formayer, H. and Kromp-Kolb, H.: Hochwasser und Klimawandel. Auswirkungen des Klimawandels auf Hochwasserereignisse in Österreich, BOKU-Met, Wien, https://meteo.boku.ac.at/klima/berichte/, 2009.

Friebe, J.: Vorarlberg. Geologie der Österreichischen Bundesländer, Verlag der Geologischen Bundesanstalt (GBA), Wien, 2007.

Gardner, W.: Some steady-state solutions of the unsaturated moisture flow equation with application to evaporation from a water table, Soil science, 85, 228–232, 1958.

Gioia, E., Speranza, G., Ferretti, M., Godt, J. W., Baum, R. L., and Marincioni, F.: Application of a process-based shallow landslide hazard model over a broad area in Central Italy, Landslides, 13, 1197–1214, doi:10.1007/s10346-015-0670-6, http://dx.doi.org/10.1007/s10346-015-0670-6, 2016.

GRASS Development Team: Geographic Resources Analysis Support System (GRASS GIS) Software, Open Source Geospatial Foundation, USA, http://grass.osgeo.org, 2014.

Hammond, C., Hall, D., Miller, S., and Swetik, P.: Level I stability analysis (LISA) documentation for version 2.0, Intermountain Research Station, Ogden, 1992.

Heimsath, A. M., Dietrich, W. E., Nishiizumi, K., and Finkel, R. C.: The soil production function and landscape equilibrium, Nature, 388, 358–361, doi:10.1038/41056, http://dx.doi.org/10.1038/41056, 1997.

Heissel, W., Oberhauser, R., and Schmidegg, O.: Geologische Karte des Walgaues, Vorarlberg 1:25.000, Verlag der Geologischen Bundesanstalt (GBA), Wien, 1967.

Heumader, J.: Die Katastrophenlawinen von Galtür und Valzur am 23. und 24.2.1999 im Paznauntal/Tirol, in: Proc. of the IX International Congress Interpraevent 2000, Villach, vol. 1, pp. 397–410, 2000.

Horn, B.: Hill shading and the reflectance map, Proceedings of the IEEE, 69, 14–47, doi:10.1109/PROC.1981.11918, http://dx.doi.org/10.1109/PROC.1981.11918, 1981.

Iverson, R. M.: Landslide triggering by rain infiltration, Water Resources Research, 36, 1897–1910, doi:10.1029/2000WR900090, http://dx.doi.org/10.1029/2000WR900090, 2000.

Kienholz, H.: Kombinierte geomorphologische Gefahrenkarte 1:10 000 von Grindelwald, {CATENA}, 3, 265–294, doi:10.1016/0341-8162(77)90034-0, http://dx.doi.org/10.1016/0341-8162(77)90034-0, 1977.

Kim, D., Im, S., Lee, C., and Woo, C.: Modeling the contribution of trees to shallow landslide development in a steep, forested watershed, Ecological Engineering, 61, Part C, 658–668, doi:10.1016/j.ecoleng.2013.05.003, http://dx.doi.org/10.1016/j.ecoleng.2013.05.003, 2013.

Kromp-Kolb, H., Nakicenovic, N., Seidl, R., Steininger, K., Ahrens, B., Auer, I., Baumgarten, A., Bednar-Friedl, B., Eitzinger, J., Foelsche, U., Formayer, H., Geitner, C., Glade, T., Gobiet, A., Grabherr, G., Haas, R., Haberl, H., Haimberger, L., Hitzenberger, R., König, M., Köppl, A., Lexer, M., Loibl, W., Molitor, R., Moshammer, H., Nachtnebel, H.-P., Prettenthaler, F., Rabitsch, W., Radunsky, K., Schneider, L., Schnitzer, H., Schöner, W., Schulz, N., Seibert, P., Stagl, S., Steiger, R., Stötter, H., Streicher, W., and Winiwarter, W.: Österreichischer Sachstandsbericht Klimawandel 2014 (AAR14). Austrian Panel on Climate Change (APCC), Verlag der Österreichischen Akademie der Wissenschaften, Wien, Österreich, 2014.

Kutschera, L. and Lichtenegger, E.: Wurzelatlas europäischer Waldbäume, 2002.

Lanni, C., Borga, M., Rigon, R., and Tarolli, P.: Modelling shallow landslide susceptibility by means of a subsurface flow path connectivity index and estimates of soil depth spatial distribution, Hydrology and Earth System Sciences, 16, 3959–3971, doi:10.5194/hess-16-3959-2012, http://dx.doi.org/10.5194/hess-16-3959-2012, 2012.

Lanni, C., McDonnell, J., Hopp, L., and Rigon, R.: Simulated effect of soil depth and bedrock topography on near-surface hydrologic response and slope stability, Earth Surface Processes and Landforms, 38, 146–159, doi:10.1002/esp.3267, http://dx.doi.org/10.1002/esp.3267, 2013.

Lateltin, O., Haemmig, C., Raetzo, H., and Bonnard, C.: Landslide risk management in Switzerland, Landslides, 2, 313–320, doi:10.1007/s10346-005-0018-8, http://dx.doi.org/10.1007/s10346-005-0018-8, 2005.

Lu, N. and Godt, J. W.: Hillslope hydrology and stability, Cambridge University Press, 2013.

Markart, G., Perzl, F., Kohl, B., Luzian, R., Kleemayr, K., Ess, B., and Mayerl, J.: Schadereignisse 22./23. August 2005 - Ereignisdokumentation und -analyse in ausgewählten Gemeinden Vorarlbergs, in: BFW-Dokumentation, vol. 5, Bundesforschungs-und Aubildungszentrum für Wald, Naturgefahren und Landschaft, Wien, 2007.

Milledge, D. G., Griffiths, D. V., Lane, S. N., and Warburton, J.: Limits on the validity of infinite length assumptions for modelling shallow landslides, Earth Surface Processes and Landforms, 37, 1158–1166, doi:10.1002/esp.3235, http://dx.doi.org/10.1002/esp.3235, 2012.

Montgomery, D. R. and Dietrich, W. E.: A Physically-based Model For the Topographic Control On Shallow Landsliding, Water Resources Research, 30, 1153–1171, doi:10.1029/93WR02979, http://dx.doi.org/10.1029/93WR02979, 1994.

Oberhauser, R.: Geologische Karte St. Gallen Süd und Dornbirn Süd 1:25.000, Verlag der Geologischen Bundesanstalt (GBA), Wien, 1982.

Oberhauser, R.: Erläuterungen zur geologisch-tektonischen Übersichtskarte von Vorarlberg 1: 200.000, Verlag der Geologischen Bundesanstalt (GBA), Wien, 1998.

ÖNORM EN ISO 22476-2:2012: Geotechnische Erkundung und Untersuchung – Felduntersuchungen – Teil 2: Rammsondierungen, 2012.

Park, D. W., Nikhil, N. V., and Lee, S. R.: Landslide and debris flow susceptibility zonation using TRIGRS for the 2011 Seoul landslide event, Natural Hazards and Earth System Sciences Discussions, 1, 2547–2587, doi:10.5194/nhessd-1-2547-2013, http://dx.doi.org/10.5194/nhessd-1-2547-2013, 2013.

Prinz, H. and Strauß, R.: Ingenieurgeologie, vol. 5, Springer, Heidelberg, 2011.

Python Software Foundation: Python Programming Language, Python Software Foundation, Hampton, New Hampshire, http://www.python.org/, 2016.

R Core Team: R: A Language and Environment for Statistical Computing, R Foundation for Statistical Computing, Vienna, Austria, https://www.R-project.org/, 2016.

Rowe, P. W. and Barden, L.: A new consolidation cell, Geotechnique, 16, 162–170, doi:10.1680/geot.1966.16.2.162, http://dx.doi.org/10.1680/geot.1966.16.2.162, 1966.

Salciarini, D., Godt, J. W., Savage, W. Z., Conversini, P., Baum, R. L., and Michael, J. A.: Modeling regional initiation of rainfall-induced shallow landslides in the eastern Umbria Region of central Italy, Landslides, 3, 181–194, doi:10.1007/s10346-006-0037-0, http://dx.doi.org/10.1007/s10346-006-0037-0, 2006.

Sass, O.: Bedrock detection and talus thickness assessment in the European Alps using geophysical methods, Journal of Applied Geophysics, 62, 254–269, doi:10.1016/j.jappgeo.2006.12.003, http://dx.doi.org/10.1016/j.jappgeo.2006.12.003, 2007.

Schmidt, H.-H., Buchmaier, R. F., and Vogt-Breyer, C.: Grundlagen der Geotechnik: Geotechnik nach Eurocode, Springer Fachmedien Wiesbaden, Heidelberg, 2014.

Schwarz, M., Preti, F., Giadrossich, F., Lehmann, P., and Or, D.: Quantifying the role of vegetation in slope stability: A case study in Tuscany (Italy), Ecological Engineering, 36, 285–291, doi:10.1016/j.ecoleng.2009.06.014, http://dx.doi.org/10.1016/j.ecoleng.2009.06.014, 2010.

Schwarz, M., Cohen, D., and Or, D.: Spatial characterization of root reinforcement at stand scale: Theory and case study, Geomorphology, 171–172, 190–200, doi:10.1016/j.geomorph.2012.05.020, http://dx.doi.org/10.1016/j.geomorph.2012.05.020, 2012.

Segoni, S., Rossi, G., and Catani, F.: Improving basin scale shallow landslide modelling using reliable soil thickness maps, Natural Hazards, 61, 85–101, doi:10.1007/s11069-011-9770-3, http://dx.doi.org/10.1007/s11069-011-9770-3, 2012.

Seibert, P., Frank, A., and Formayer, H.: Synoptic and regional patterns of heavy precipitation in Austria, Theoretical and Applied Climatology, 87, 139–153, doi:10.1007/s00704-006-0198-8, http://dx.doi.org/10.1007/s00704-006-0198-8, 2007.

Srivastava, R. and Yeh, T. C. J.: Analytical Solutions For One-dimensional, Transient Infiltration Toward the Water-table In Homogeneous and Layered Soils, Water Resources Research, 27, 753–762, doi:10.1029/90WR02772, http://dx.doi.org/10.1029/90WR02772, 1991.

Steinacher, R., Medicus, G., Fellin, W., and Zangerl, C.: The Influence of Deforestation On Slope (in-) Stability, Austrian Journal of Earth Sciences, 102, 90–99, 2009.

Tang, Y., Reed, P., Wagener, T., and van Werkhoven, K.: Comparing sensitivity analysis methods to advance lumped watershed model identification and evaluation, Hydrology and Earth System Sciences, 11, 793–817, doi:10.5194/hess-11-793-2007, http://dx.doi.org/10.5194/hess-11-793-2007, 2007.

Tesfa, T. K., Tarboton, D. G., Chandler, D. G., and McNamara, J. P.: Modeling soil depth from topographic and land cover attributes, Water Resources Research, 45, W10 438, doi:10.1029/2008WR007474, http://dx.doi.org/10.1029/2008WR007474, 2009.

USGS: TRIGRS 2.0. Accessed on 02 Nov 2016, http://pubs.usgs.gov/of/2008/1159/downloads/, 2016.

van Bebber, W. J.: Die Zugstrassen der barometrischen Minima nach den Bahnenkarten der Deutschen Seewarte für den Zeitraum von 1870–1890, Meteorologische Zeitschrift, 8, 361–366, 1891.

van Westen, C. J., van Asch, T. W. J., and Soeters, R.: Landslide hazard and risk zonation - why is it still so difficult?, Bulletin of Engineering Geology and the Environment, 65, 167–184, doi:10.1007/s10064-005-0023-0, http://dx.doi.org/10.1007/s10064-005-0023-0, 2006.

Vieira, B. C., Fernandes, N. F., and Filho, O. A.: Shallow landslide prediction in the Serra do Mar, Sao Paulo, Brazil, Natural Hazards and Earth System Sciences, 10, 1829–1837, doi:10.5194/nhess-10-1829-2010, http://dx.doi.org/10.5194/nhess-10-1829-2010, 2010.

Wagener, T. and Kollat, J.: Numerical and visual evaluation of hydrological and environmental models using the Monte Carlo analysis toolbox, Environmental Modelling & Software, 22, 1021–1033, doi:10.1016/j.envsoft.2006.06.017, http://dx.doi.org/10.1016/j.envsoft.2006.06.017, 2007.

Werner, R. and Auer, I.: Klima von Vorarlberg: Eine anwendungsorientierte Klimatographie. 2. Niederschlag und Gewitter, Schnee und Gletscher, Verdunstung, Luftdruck, Wind, Umweltinstitut des Landes Vorarlberg, Bregenz, 2001a.

Werner, R. and Auer, I.: Klima von Vorarlberg: Eine anwendungsorientierte Klimatographie. 1. Lufttemperatur, Bodentemperatur, Wassertemperatur, Luftfeuchte, Bewölkung, Nebel, Umweltinstitut des Landes Vorarlberg, Bregenz, 2001b.

Wiedenhöft, A. and Vatslid, S.: LiDAR und RGB - Land Vorarlberg. Technischer Abschlussbericht., Tech. rep., Trimble Germany GmbH, 2014.

Wiegand, C., Kringer, K., Geitner, C., and Rutzinger, M.: Regolith structure analysis - A contribution to understanding the local occurrence of shallow landslides (Austrian Tyrol), Geomorphology, 183, 5–13, doi:10.1016/j.geomorph.2012.06.027, http://dx.doi.org/10.1016/j.geomorph.2012.06.027, 2013.

Wood, J.: The geomorphological characterisation of digital elevation models, Ph.D. thesis, University of Leicester, http://www.soi.city.ac.uk/~jwo/phd, 1996.

Zieher, T., Perzl, F., Rössel, M., Rutzinger, M., Meißl, G., Markart, G., and Geitner, C.: A multi-annual landslide inventory for the assessment of shallow landslide susceptibility - Two test cases in Vorarlberg, Austria, Geomorphology, 259, 40–54, doi:10.1016/j.geomorph.2016.02.008, http://dx.doi.org/10.1016/j.geomorph.2016.02.008, 2016.

Zieher, T., Markart, G., Ottowitz, D., Römer, A., Rutzinger, M., Meißl, G., and Geitner, C.: Water content dynamics at plot scale–comparison of time-lapse electrical resistivity tomography monitoring and pore pressure modelling, Journal of Hydrology, 544, 195–209, doi:10.1016/j.jhydrol.2016.11.019, http://dx.doi.org/10.1016/j.jhydrol.2016.11.019, 2017.

Zizioli, D., Meisina, C., Valentino, R., and Montrasio, L.: Comparison between different approaches to modeling shallow landslide susceptibility: a case history in Oltrepo Pavese, Northern Italy, Natural Hazards and Earth System Science, 13, 559–573, doi:10.5194/nhess-13-559-2013, http://dx.doi.org/10.5194/nhess-13-559-2013, 2013.